LA-UR-15-24324
Approved for public release; distribution is unlimited.

Title:	Fuel Fabrication Capability WBS 01.02.01.05 – HIP Bonding Experiments Final Report
Author(s):	Dickerson, Patricia O'Donnell; Summa, Deborah Ann; Liu, Cheng; Tucker, Laura Arias; Chen, Ching-Fong; Aikin, Beverly; Aragon, Daniel Adrian; Beard, Timothy Vance; Montalvo, Joel Dwayne; Pena, Maria Isela; Dombrowski, David E.
Intended for:	Report
Issued:	2015-06-10

Fuel Fabrication Capability WBS 01.02.01.05 – HIP Bonding Experiments
Final Report

Pat Dickerson, Deb Summa, Cheng Liu, Laura Tucker, Chris Chen, Beverly Aikin, Daniel Aragon, Tim Beard, J.D. Montalvo, Maria Pena, and Dave Dombrowski

Materials Science and Technology Division
Los Alamos National Laboratory, Los Alamos, NM 87545

Objectives

The goals of this project were to demonstrate reliable, reproducible solid state bonding of aluminum 6061 alloy plates together to encapsulate DU-10 wt% Mo surrogate fuel foils. This was done as part of the CONVERT Fuel Fabrication Capability effort in Process Baseline Development . Bonding was done using Hot Isotatic Pressing (HIP) of evacuated stainless steel cans (a.k.a HIP cans) containing fuel plate components and strongbacks. Gross macroscopic measreurements of HIP cans prior to HIP and after HIP were used as part of this demonstration, and were used to determine the accuracy of a finitie element model of the HIP bonding process. The quality of the bonding was measured by controlled miniature bulge testing for Al-Al, Al-Zr, and Zr-DU bonds. A special objective was to determine if the HIP process consistently produces good quality bonding and to determine the best characterization techniques for technology transfer.

1.0 Background

This activity investigates the HIP bonding process utilized to bond the aluminum alloy 6061 cladding to the Zr-sheathed U-10Mo monolithic foils prepared by Idaho national Laboratory [1] under WBS 01.02.01.04 - Cold Rolling Experiments as part of the Fuel Fabrication Capability program's WBS 01.02.01 - Process Baseline Development effort. The series of experiments conducted here will aid overall demonstration of the hot isostatic pressing (HIP) process and material continuity. INL has shown over hundreds of mini plate irradiation tests what set of HIP process conditions (temperature and pressure) result in a satisfactory aluminum to aluminum bond. This bond is based on fundamentals of atomic diffusion and these fundamentals show that aluminum interface surface quality, pressure perpendicular to the bonding interface and bonding temperature control bond strength. U-10Mo metallurgical characteristics will have secondary or tertiary effects on aluminum to aluminum diffusion bonding since the aluminum to aluminum interfaces do not include U-Mo. Therefore it is only necessary to demonstrate process reproducibility with some consistent subset of U-10Mo foils produced in WBS 1.2.1.4.

The robustness of HIP cladding was completed by cladding two different U-10Mo foil thicknesses with two different 6061 aluminum cladding thicknesses. The intent is to use two extremes from the range of foil and cladding thicknesses that was produced with this process. Successful bonding of these different geometrical sets will demonstrate the robustness of the process for the U.S. High Performance Research Reactor fuels.

These tests were used to demonstrate the typical surface finish and flatness of the HIPped plates. These characteristics are important to downstream processing and help define the costs of downstream processing. There is a balance to be struck between minimizing costs of downstream processing such as machining and preserving the minimum cladding thickness. These tests are based on the best available data on this balance at this time. While net shape HIPped plates may be practical after long term process optimization, there is not sufficient data at present to assume that for these tests.

2.0 Results and Discussion

2.1 Fuel Plates

LANL received LEU plates from INL and the dimensions and compositional information. Table 1 summaries the project ID, unique ID, batch number, description, gross weight, net weight DU weight, DU-235 weight, %DU content, and %DU enrichment. These plates have been assigned to specific programs and natures of those projects such as rolling, HIP, canless HIP, etc.

Table 1: The project ID, unique ID, batch number, description, gross weight, net weight DU weight, DU-235 weight, %DU content, and %DU enrich.

Comments	Project ID	Unique ID	BATCH NUMBER	Description	GROSS WT (g)	Net WT (g)	DU WT (g)	DU-235 WT (g)	%DU content	%DU Enrich
LANL 1	Alloy 548	A-548-1	140-60-60336-61428	Sheared Zr Co-Rolled Du10 Mo FFC LANL Foil Alloy 548-1	421.696	402.037	364.165	0.634	90.58%	0.17%
LANL 1	Alloy 548	A-548-2	140-60-60336-61428	Sheared Zr Co-Rolled Du10 Mo FFC LANL Foil Alloy 548-2	429.162	409.155	370.613	0.645	90.58%	0.17%
LANL 1	Alloy 549	A549-1	140-60-60336-61428	Sheared Zr Co-Rolled Du10 Mo FFC LANL Foil Alloy 549	430.755	410.714	363.613	0.88	88.53%	0.24%
LANL 1	Alloy 549	A549-2	140-60-60336-61428	Sheared Zr Co-Rolled Du10 Mo FFC LANL Foil Alloy 549	445.996	425.245	376.478	0.911	88.53%	0.24%
LANL 1	Alloy 550	A-550-1	140-60-60336-61428	Zr Co-Rolled Du10 Mo FFC LANL Foil Alloy 550-1	441.715	422.516	374.062	0.905	88.53%	0.24%
LANL 1	Alloy 545	A-545-1	140-60-60336-61436	Sheared Zr Co-Rolled Du10 Mo FFC LANL Foil Alloy 545-1	426.648	407.433	366.901	0.653	90.05%	0.18%
LANL 1	Alloy 545	A-545-2	140-60-60336-61436	Sheared Zr Co-Rolled Du10 Mo FFC LANL Foil Alloy 545-2	443.86	423.869	381.703	0.679	90.05%	0.18%
LANL 1	Alloy 543	A-543-1	140-60-60336-61428	Sheared Zr Co-Rolled Du10 Mo FFC LANL Foil Alloy 543	422.956	404.059	364.065	0.652	90.10%	0.18%
LANL 1	Alloy 543	A-543-2	140-60-60336-61428	Sheared Zr Co-Rolled Du10 Mo FFC LANL Foil Alloy 543	426.533	407.476	367.144	0.657	90.10%	0.18%
LANL 1	Alloy 544	A-544-1	140-60-60336-61428	Sheared Zr Co-Rolled Du10 Mo FFC LANL Foil Alloy 544-1	415.357	396.732	357.463	0.640	90.10%	0.18%
LANL 1	Alloy 546	A-546-1	140-60-60336-61428	Sheared Zr Co-Rolled Du10 Mo FFC LANL Foil Alloy 546-1	432.611	413.181	372.078	0.662	90.05%	0.18%
LANL 1	Alloy 547	A-547-1	140-60-60336-61428	Sheared Zr Co-Rolled Du10 Mo FFC LANL Foil Alloy 547-1	446.755	426.020	385.889	0.671	90.58%	0.17%
LANL 2	Alloy 532	A-532-2	140-60-60336-61428	Sheared Zr Co-Rolled Du10 Mo FFC LANL Foil Alloy 532-2	152.924	138.075	123.458	0.280	89.41%	0.23%
LANL 2	Alloy 527	A-527-1	140-60-60336-61428	Sheared Zr Co-Rolled Du10 Mo FFC LANL Foil Alloy 527-1	168.851	152.413	134.219	0.238	88.06%	0.18%
LANL 2	Alloy 527	A-527-2	140-60-60336-61428	Sheared Zr Co-Rolled Du10 Mo FFC LANL Foil Alloy 527-2	121.904	110.036	96.901	0.172	88.06%	0.18%
LANL 2	Alloy 528	A-528-1	140-60-60336-61428	Sheared Zr Co-Rolled Du10 Mo FFC LANL Foil Alloy 528-1	143.221	129.824	114.327	0.202	88.06%	0.18%
LANL 2	Alloy 528	A-528-2	140-60-60336-61428	Sheared Zr Co-Rolled Du10 Mo FFC LANL Foil Alloy 528-2	124.27	112.646	99.199	0.176	88.06%	0.18%
LANL 2	Alloy 529	A-529-1	140-60-60336-61428	Sheared Zr Co-Rolled Du10 Mo FFC LANL Foil Alloy 529-1	164.124	148.799	131.037	0.232	88.06%	0.18%
LANL 2	Alloy 530	A-530-1	140-60-60336-61428	Sheared Zr Co-Rolled Du10 Mo FFC LANL Foil Alloy 530-1	169.822	153.784	135.427	0.240	88.06%	0.18%
LANL 2	Alloy 531	A-531-1	140-60-60336-61428	Sheared Zr Co-Rolled Du10 Mo FFC LANL Foil Alloy 531-1	173.947	157.595	140.912	0.320	89.41%	0.23%
LANL 2	Alloy 531	A-531-2	140-60-60336-61428	Sheared Zr Co-Rolled Du10 Mo FFC LANL Foil Alloy 531-2	123.986	112.331	100.439	0.228	89.41%	0.23%
LANL 2	Alloy 533	A-533-1	140-60-60336-61428	Sheared Zr Co-Rolled Du10 Mo FFC LANL Foil Alloy 533-1	178.329	161.401	144.315	0.328	89.41%	0.23%
LANL 2	Alloy 533	A-533-2	140-60-60336-61428	Sheared Zr Co-Rolled Du10 Mo FFC LANL Foil Alloy 533-2	124.049	112.273	100.388	0.228	89.41%	0.23%
LANL 3	Alloy 522	A-522	140-60-60336	Zr Co-Rolled Du10 Mo FFC LANL Foil Alloy 522	155.392	144.356	129.893	0.244	89.98%	0.19%
LANL 3	Alloy 525	A-525	140-60-60336	Zr Co-Rolled Du10 Mo FFC LANL Foil Alloy 525	183.758	169.047	153.604	0.309	90.87%	0.20%
LANL 4	Alloy 535	A-535-1	140-60-60336-61436	Sheared Zr Co-Rolled Du10 Mo FFC LANL Foil Alloy 535-1	404.926	387.796	346.450	0.637	89.34%	0.18%
LANL 4	Alloy 538	A-538-1	140-60-60336-61436	Sheared Zr Co-Rolled Du10 Mo FFC LANL Foil Alloy 538-1	439.875	420.569	381.692	0.767	90.76%	0.20%
LANL 4	Alloy 542	A-542-1	140-60-60336-61436	Sheared Zr Co-Rolled Du10 Mo FFC LANL Foil Alloy 542-1	440.605	424.606	384.991	0.770	90.67%	0.20%
LANL 4	Alloy 540	A-540-1	140-60-60336-61436	Sheared Zr Co-Rolled Du10 Mo FFC LANL Foil Alloy 540-1	434.163	415.799	373.118	0.746	89.74%	0.20%
LANL 4	Alloy 540	A-540-2	140-60-60336-61436	Sheared Zr Co-Rolled Du10 Mo FFC LANL Foil Alloy 540-2	214.357	205.290	184.217	0.368	89.74%	0.20%
LANL 4	Alloy 536	A-536-1	140-60-60336-61436	Sheared Zr Co-Rolled Du10 Mo FFC LANL Foil Alloy 536-1	433.594	415.211	372.59	0.749	89.74%	0.20%
LANL 4	Alloy 536	A-536-2	140-60-60336-61436	Sheared Zr Co-Rolled Du10 Mo FFC LANL Foil Alloy 536-2	331.632	317.572	284.973	0.573	89.74%	0.20%
LANL 4	Alloy 537	A-537-1	140-60-60336-61436	Sheared Zr Co-Rolled Du10 Mo FFC LANL Foil Alloy 537-1	328.510	314.487	282.205	0.567	89.74%	0.20%
LANL 4	Alloy 537	A-537-2	140-60-60336-61436	Sheared Zr Co-Rolled Du10 Mo FFC LANL Foil Alloy 537-2	271.670	260.073	233.376	0.469	89.74%	0.20%
LANL 4	Alloy 539	A-539-1	140-60-60336-61436	Sheared Zr Co-Rolled Du10 Mo FFC LANL Foil Alloy 539-1	434.649	415.860	373.172	0.746	89.74%	0.20%
LANL 4	Alloy 539	A-539-2	140-60-60336-61436	Sheared Zr Co-Rolled Du10 Mo FFC LANL Foil Alloy 539-2	209.426	200.373	179.805	0.360	89.74%	0.20%
				Total	**11112**	**10528.7**	**9444.88**	**18.539**		

2.2 HIP Bond Process

In FY2014, three cans were HIPped at LANL. In FY2015, the balance of the cans were HIPped, which is a total of 6 cans with a total of 24 foils. The stainless steel HIP can had been designed using lessons learned from INL[2] and LANL[3-5] . Figure 1 is a schematic showing the designs of (A) HIP can baseline design.(B) Al cladding with deep pocket and U-10Mo assembly and (C) Al cladding with shallow pocket and U-10Mo assembly. Each HIP can was filled with an assembly consisting of DU-10Mo foils, strongbacks (Grade 01 tool steel) and a parting agent down selected from FY 11 experiments (WBS 1.2.3.3). All strongbacks and aluminum cladding are straight and flat. Total thickness of each aluminum cladding and foil set was 0.70 in. Each aluminum cladding set will have a top cladding piece that is 0.38 in. thick and a bottom cladding plate that is 0.32 in. thick. These dimensions are intermediate between those used for mini plate tests at INL and AFIP size tests at B&W. Because a standard set of upper and lower cladding pieces were used, thinner foils have a greater cladding thickness in the HIP can assembly than thicker foils.

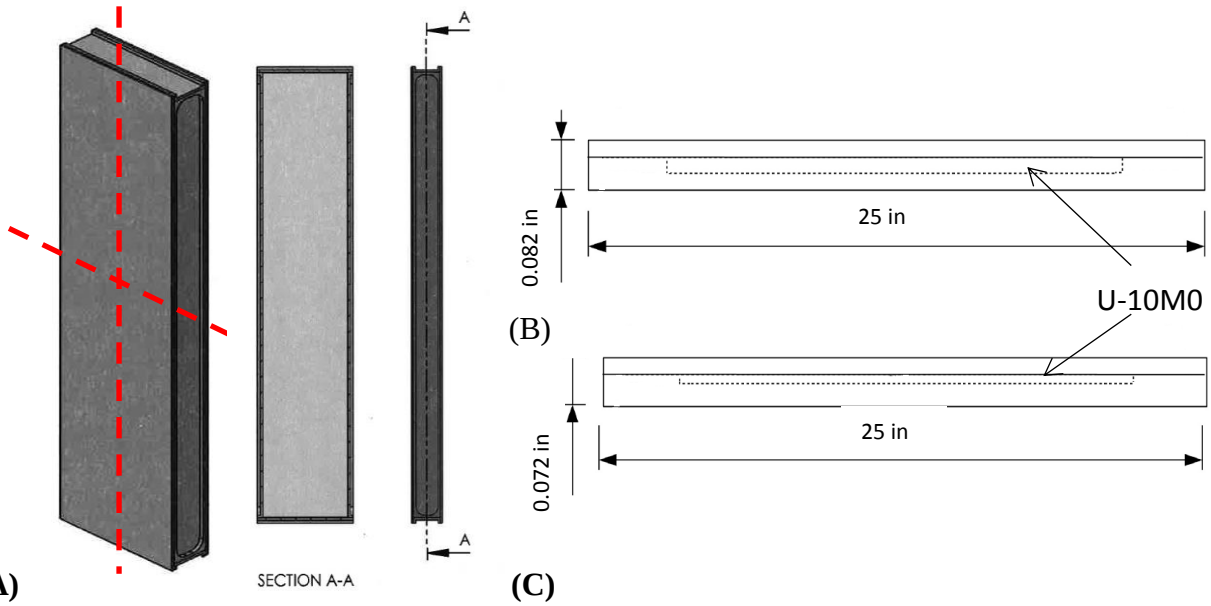

Figure 1: A schematic showing the designs of (A) HIP can baseline design.(B) Al cladding with deep pocket and U-10Mo assembly and (C) Al cladding with shallow pocket and U-10Mo assembly.

The interior of the HIP can and all metallic components are cleaned using a standard procedure qualified by surface science measurements, especially angle resolved photoelectron spectroscopy (WBS 1.2.3.9). The cleaning processes described below were developed in the LANL MST-6 Sigma Cleaning Facility [6]. This facility exists for precision cleaning and surface finishing of nonnuclear and nuclear materials and parts. In general, cleaning processes in this facility are developed from best practices in the industry, along with experience of cleaning and surface finishing experts. Within the scope of cleaning processes readily implemented or already available in the facility, new methods were developed for cleaning the various materials surfaces

in this program, particularly for those materials and surfaces going into a bonding operation where cleanliness is paramount in forming a strong coherent interfacial bond. These cleaning processes were designed to be as efficient and effective as possible for the large area foils required for this program.

If there are permanent marker (sharpie) or other lettering or marks on any metal surface, these need to be removed with solvent or by other means prior to the aqueous cleaning processes described below. Clean stable storage after cleaning process operations involve wrapping the metal part in UHV aluminum foil (this foil is obtained certified as carefully cleaned of any surface contaminants used in its manufacture). This storage method is sufficient for relatively long term storage of the Stainless Steel, Carbon Steel, Tool Steel, Zr foil, Zr clad U10%Mo fuel, and 6061 Al in a dry location. Storage of the bare U10%Mo LEU fuel foil for extended periods of time (>1 day) requires more rigorous measures, especially in a humid environment. Cleaning processes take place at ambient (room) temperature unless otherwise noted. Cleaning operations should take place in a clean environment nominally free of dirt or dust. Aqueous cleaning solutions should be prepared with high quality deionized water. Inert (non-reactive) fixtures should be used for handling and immersion of metal parts. Clean gloves should be used to handle cleaned parts. The cleaning procedures for each individual component are described as follows.

A. Stainless Steel cleaning procedure
Used as HIP can fabrication material or as a welded HIP can
Stainless steel as manufactured or as machined surface
1. Ultrasonic Blue Gold Cleaner at 60°C for 6 minutes
2. Immerse in Caustic 10% NaOH 60°C for 6 minutes
3. DI water rinse 30 seconds over full part
4. Immerse in 50% HNO3 for 6 minutes
5. DI water rinse 30 seconds over full part
6. Clean compressed nitrogen gas dry

B. Carbon (mild) Steel cleaning procedure
Used to fabricate co-rolling cans
Used as formed (drawn) HIP cans
Carbon Steel as manufactured or as machined surface
1. If rust or scale is present on surface, clean in 10% sulfuric acid and/or 50% hydrochloric acid as required
2. Ultrasonic Blue Gold Cleaner at 60°C for 6 minutes
3. DI water rinse 30 seconds over full part
4. Clean compressed nitrogen gas dry

C. Tool Steel cleaning procedure
Used as strongback plates inside of HIP cans
Tool Steel as machined surface
1. If rust or scale is present on surface, clean in 10% sulfuric acid and/or 50% hydrochloric acid as required
2. Ultrasonic Blue Gold Cleaner at 60°C for 6 minutes

3. DI water rinse 30 seconds over full part
4. Clean compressed nitrogen gas dry

D. U10%Mo fuel material cleaning procedure
Fuel meat prior to Zr roll cladding operation
U10%Mo fuel foil/plate with machined finish
1. Ultrasonic Blue Gold Cleaner at 60°C for 6 minutes
2. Immerse in Caustic 10% NaOH 60°C for 6 minutes
3. Immerse in 50% HNO3 for 6 minutes
4. Repeat 2+3 if oxide scale is still present
5. DI water rinse 30 seconds over full part
6. Clean compressed nitrogen gas dry

E. Zirconium foil cleaning procedure
Used in cladding operation with U10%Mo fuel meat
Zr foil/plate as manufactured or as machined
1. Ultrasonic Blue Gold Cleaner at 60°C for 2 minutes
2. DI water rinse 30 seconds over full part
3. Immerse in 50% nitric acid plus 2% ammonium bifluoride (NH4HF2) soak for 2 minutes or less (when surface becomes uniform shiny)
4. DI water rinse 30 seconds over full part
5. Clean compressed nitrogen gas dry

F. Zirconium clad U10%Mo foil cleaning procedure
Zr roll clad U10%Mo fuel meat to go into HIP operation
Zr roll clad U10%Mo foil as manufactured
1. Ultrasonic Blue Gold Cleaner at 60°C for 2 minutes
2. DI water rinse 30 seconds over full part
3. Immerse in 50% nitric acid plus 2% ammonium bifluoride (NH4HF2) soak for 2 minutes or less (when surface becomes uniform shiny)
4. DI water rinse 30 seconds over full part
5. Clean compressed nitrogen gas dry

G. Aluminum 6061 plate cleaning procedure
Used as fuel plate cladding in HIP process
Aluminum 6061 plate as manufactured or as machined
1. Ultrasonic Blue Gold cleaner at 60°C for 10 seconds only
2. DI water rinse 30 seconds over full part
3. Immerse in 50% nitric acid plus 2% ammonium bifluoride for 10 seconds
4. DI water rinse 30 seconds over full part
5. Etch in 10% sodium hydroxide at 60°C for 30 seconds
6. DI water rinse 30 seconds over full part
7. Immerse in 50% nitric acid plus 2% ammonium bifluoride for 15 seconds
8. DI water rinse 30 seconds over full part
9. Immerse in 50% nitric acid for 30 seconds to one minute.
10. DI water rinse 30 seconds over full part

11. Clean compressed nitrogen gas dry

Once cleaned, metal components were handled with gloves only and wrapped in ultrahigh vacuum aluminum foil. Once all cleaned components have been assembled into the HIP can, the final HIP can side was placed on the opening and the HIP can transported to an inert atmosphere glovebox where the final side was welded on under nitrogen atmosphere. The HIP can was placed in an oven and attached to a pumping apparatus which will degas the HIP can at 350^{o}C for ninety minutes. The degassing valve was closed, the degassing stem was mechanically crimped closed and welded. Figure 2(a) is a typical picture showing the multiple HIP cans before HIP. HIP Cans were labeled by small notches in a re-entrant space near evacuation tubes as well as indelible marker. Indelible marker tends to burn off during bake out and HIP processing of the cans. Figure 2(b) Cans after the HIP process. The bottom two cans show bulging.

The HIP can was transported to a HIP. HIP tool place at 560^{o}C and 15,000 psi for 120 minutes. Figure 2(b) shows the typical HIPped cans after the HIP process. The bottom two cans show bulging.

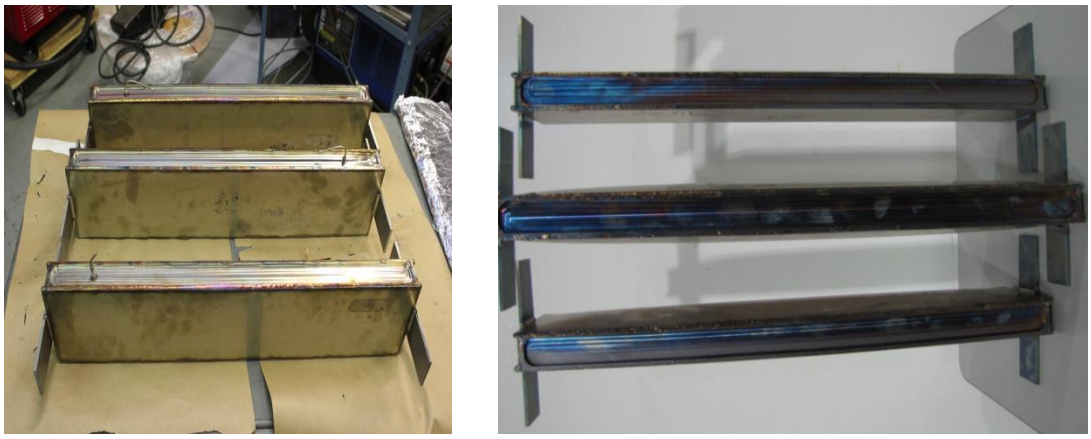

(A) **(B)**

Figure 2: (a) HIP Cans were labeled by small notches in a re-entrant space near evacuation tubes as well as indelible marker. Indelible marker tends to burn off during bake out and HIP processing of the cans. (b) Cans after the HIP process. The bottom two cans show bulging.

The HIPped can was transported to a machine shop and one end was cut off using band saw or similar device. The top of the can was also removed from the assembly. Plates were manually separated from strongbacks and any difficulty noted. Plates were photographed from front and edge for curvature. Figure 3 shows the plates from the HIP can. Plate surfaces was manually inspected for adhesion of parting agent. Molydisulfide parting agent was manually removed using acetone. As indicated in figure 3, the plate that is located in the middle of the HIP can shows the flattest shape after HIP. In contrast, the plate located at the top and bottom of the can

had a significant amount of distortion with a significant curved shape especially the bottom foil (~1.8 cm). Based on the visual inspection of the HIPped can, it is believed that the large distortion indicates that the top and bottom plates had a large displacement. The large displacement was not uniform from the edge to center. Another words, the center portion had the large movement toward the bottom while the edge had a smaller movement due to the restriction from the edge/end plates. In contrast, the bottom plate had minimal differential movement due to the thicker and more rigid bottom plate. This speculation will also be confirmed with the finite element analysis in the next section. Based on this observation, it is highly recommended to use a thinner plate to replace the thicker bottom plate as well as for the four walls, so that the whole can be collapsed from all sides with uniform pressure on to all plates. Curvature was assessed using white light interferometry. The data was input into the HIP can models developed for the HIP Can Optimization work package.

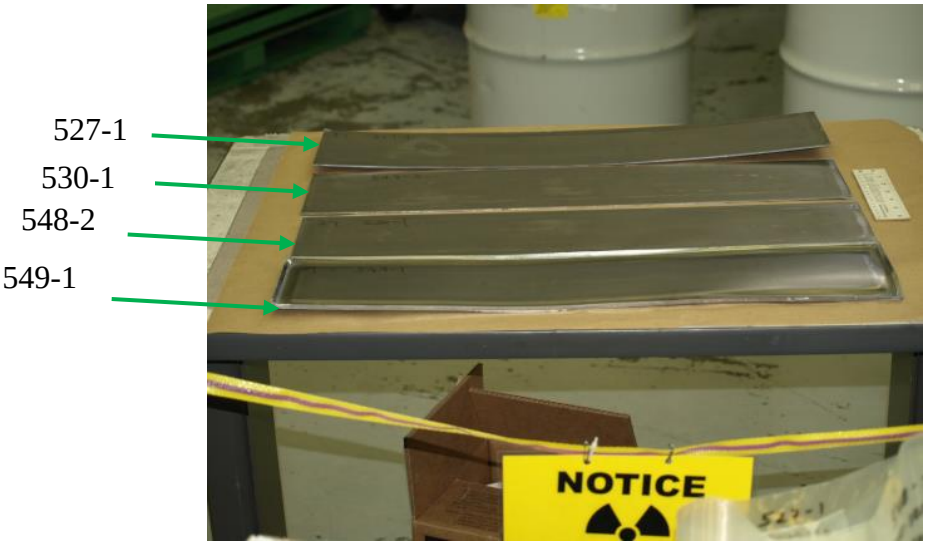

Figure 3: The plates from the HIP can. The plate that located at the bottom of the HIP can show the flattest shape after HIP. In contrast, the plate located at the top of the can had significant amount of distortion with a significant curved shape.

2.3 Finite Element Analysis (FEA)

A finite element simulation of the HIP cycle was performed on the can assembly. Abaqus 6.14 Standard was used to simulate the 2D plane strain section of the HIP can assembly with half-symmetry. To accurately simulate the HIP cycles, an average of ten successful experimental HIP runs were used as the input conditions for temperature and pressure of the FEA. Figure 4(a) shows the average pressure and temperature profile which was entered as amplitude profiles with respect to time increments. The HIP cycle consists of three stages: heating and pressurization, holding, and cooling and depressurization. Figure 4(b) summarizes the stages of the HIP cycle.

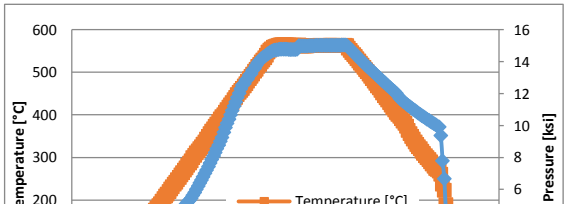

Stages	Time [min]	Temp. [ºC]	Pressure [ksi]
Heating and Pressurization	175	RT to 560	atm to 15
Holding	90	560	15
Cooling and Depressurization	200	560 to RT	15 to atm

(a) **(b)**

Figure 4: (a) Averaged HIP cycle runs. (b) Stages of the HIP cycle.

An elasto-platic temperature-dependent material model was used in the fully coupled transient temperature displacement analysis was used to simulate the hot isostatic pressing process. The HIP can assembly is shown in Figure 5. The assembly consists of a SS304L can, cover, and end plate (represented in dark grey), five 1010 steel strongbacks (represented by light grey), and four Al6061 cladding with alternating shallow and deep pockets (represented by yellow). The deep pockets are filled with U-10 Mo plates (represented by red). The exterior surface of the can, cover, and end plate are the surfaces where the temperature and pressure amplitude profile were applied. A surface-to-surface contact formulation with finite sliding interaction was applied to all the surfaces in contact during the simulation. Thermal conductance, normal behavior, and tangential behavior with a coefficient of friction of 0.3 were applied to all the surfaces in contact. CPE4RT 4-node plate strain thermally coupled quadrilateral, bilinear, reduced integration with hourglass control were used for the can and fuel foil.

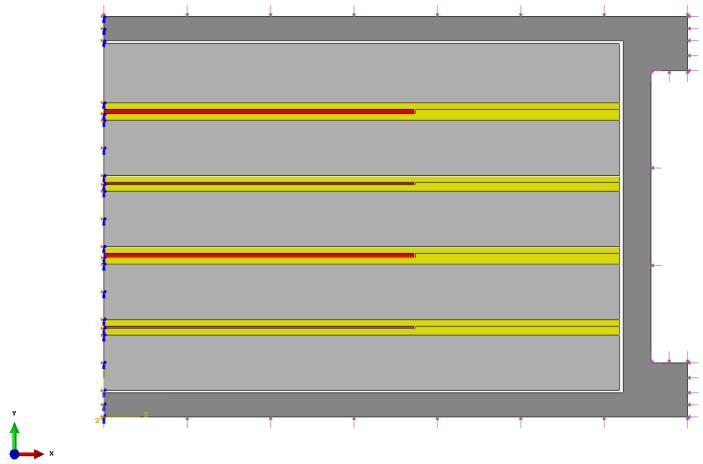

Figure 5: Schematic representation of the HIP can assembly showing the boundary conditions applied to the model. Pink arrows on the outer surface represent the application of the hot isostatic pressure and temperature. The bolded blue arrows on the vertical axis represents the half-symmetry constraint.

The mechanical and thermal properties with respect to temperatures for each material are summarized in Table 2. An extended range of temperature- dependent data spanning the loading

range is embedded into the material model but are not included in the report for clarity and brevity.

A)

	Yield [MPa]	Tensile [MPa]	Elong. [%]	Young Modulus [GPa]	Poisson's ratio	Temp. [°C]
Al6061	276	310	12	69	0.33	25
	12	24	95	-	-	371
1010 Steel	210	330	43	200	0.28	25
	100	120	20	-	-	600
SS304L	215	505	70	193	0.3	25
	156	346	40	-	-	315
U10Mo	780	889	10	65	0.35	25
	427	455	2.6	-	-	600

B)

	Thermal Expansion [1/K]	Thermal Conductivity [W/m K]	Specific heat [J/Kg K]	Temp. [°C]
Al6061	2.36E-05	179.6	896	25
	2.54E-05	175	1126	581
1010 Steel	1.26E-05	57.8	481	25
	1.46E-05	36.8	754	600
SS304L	1.73E-05	16.27	456	25
	1.87E-05	24.46	586	560
U10Mo	1.18E-05	11.3	143	25
	1.67E-05	35.5	167	600

Table 2. (a) Summary of the mechanical properties. (b) Summary of the thermal properties

Figure 6(a) shows the Von Mises stress contour plot after the HIP process. Higher stress concentration is found at the corners between the side plate and the top and bottom plate. This region is where the top and bottom plate plastically deforms filling the gaps inside the can. An even higher stress concentration area is found on the outer fuel plate assemblies, specifically where the aluminum cladding seals the U-10Mo fuel foil. The other two fuel assemblies located near the midpoint of the can do not show any high stress concentration. Figure 6(b) shows the equivalent plastic strain of the HIP can assembly. The highest amount of plastic deformation is located in the aluminum cladding which surrounds the U-10Mo fuel foils giving a sealed fuel foil assembly.

After the HIP cycle external cross section dimensions were measured at the ends of the can and three equally spaced intermediate positions of 3 different can assemblies. Figure 7(a) shows the experimental measurements of a representative HIP can assembly. Measurements were compared at the exact location with the FEA model. Measurements from experiment show the can is approximately 0.0028” thicker across the width than predicted by simulation. Figure 7 (b) shows the comparison table between the experimental measurements and the FEA predicted dimensions. The simulation predicts increased thickness in the joint between the top/bottom plate and the side plate. The FEA does not take into consideration the height of the MoS_2 sprayed between the strong backs and aluminum cladding. The model predicted results will be used as a guide to narrow down the micrograph and microhardness sample area selections.

(a)

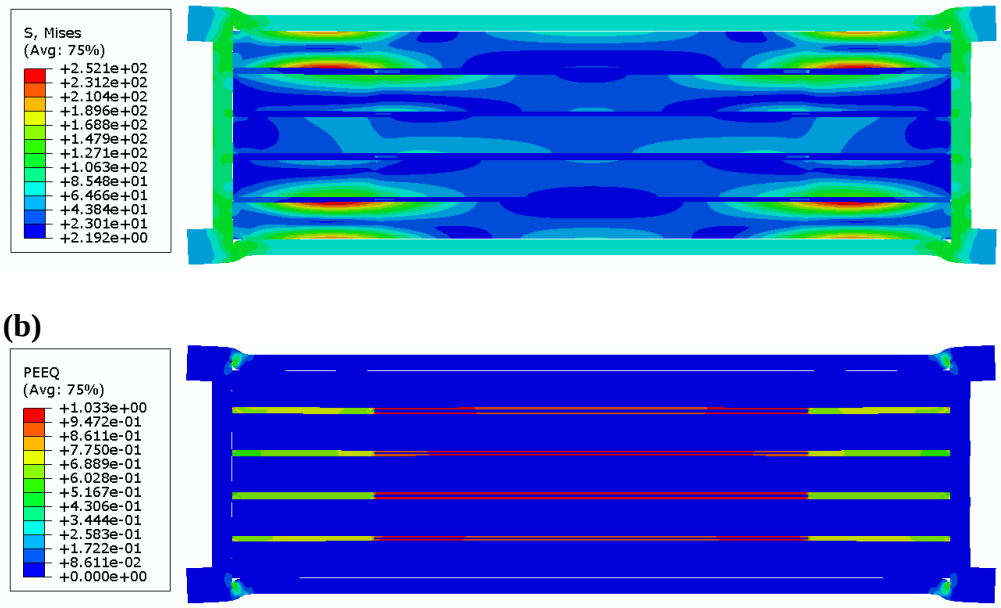

Figure 6: (a) Von Mises stress countouplot and (b) Equicalent plastic strain of the HIP can assembly after the three stages of hot isostatic pressing.

(a)

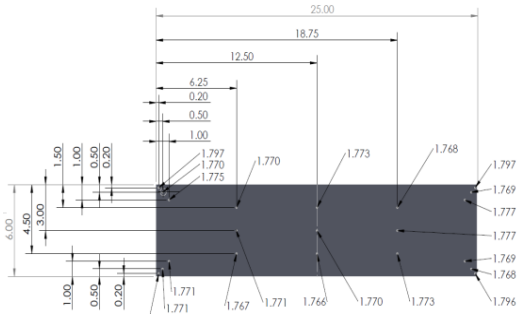

(b)

Location from edge	Can measurements [inch]	FEA dimensions [inch]	Can measurements - FEA dimension [inch]
0.20”	**1.7965**	**1.802**	**-0.0055**
0.50”	**1.7695**	**1.778**	**-0.0085**
1”	1.773	1.7676	0.0054
1.50”	1.7695	1.7678	0.0017
3”	1.7713	1.7671	0.0042

Figure 7: (a) Experimental measurement of a representative HIP can assembly (b) Table of comparison between the can measurements and the FEA dimensions.

2.4 Ultrasonic Testing and Flash Thermography

Ultrasonic testing was applied to qualitatively assess bonding status and cladding thickness/uniformity. Twenty four plates from 6 HIP cans were provided. Plates were nominally 25” x 5” x 0.072 or 0.082” depending upon the fuel core insert. Although plates were intended to be flat, all exhibited some degree of bowing from end to end with the worst cases having displacements reaching up to 1.5” from the center to the end. Little to no axial twist was observed, although a number of plates did have extruded aluminum flash protruding perpendicular to the plate surface at irregular intervals along the edges. The plates had a fairly uniform, dull matte finish, not especially smooth but generally with no obvious pits, gouges or

other substantial surface defects. An acetone wipe-down prior to shipping removed most of the MoS_2 parting agent, but a fine blackish powder still rubbed off during handling and a sulphurous odor coupled with slight surface effervescence was noted when the plates remained immersed in the ultrasonic water tank for an extended period of time.

Plates were inspected using a 3-axis immersion raster scanner with encoded Cartesian stages and a 30 MHz, 0.25" diameter spherically-focused transducer oriented normal to the surface of the part, as shown in Figure 8. The water path was adjusted to center the focal zone of the transducer on the upper cladding/fuel core interface. Pulser/receiver settings were adjusted to optimize contrast, and using an interface trigger to track the front surface of the part, amplitude, time-of-flight (TOF) and full waveform data was collected at spatial intervals of 1 mm in both the x and y dimension over the entire surface of the part.

All plates were initially inspected from the front surface. The front surface is defined as the surface that is facing up when the plate is laid on the table the ends bowed up. Plate ID numbers were written on the upper left corner of the front surface of each plate. A number of plates, including all those in which potential anomalies at the front interface were identified, were inspected from the back surface as well. Plates with end to end curvature sufficient to cause interference during scanning were clamped within a welding fixture in an effort to temporarily flatten the samples for inspection. Since they were too large for the fixture, plates were clamped along the bottom and left edges with the upper and right edges free. In this arrangement the upper edge and especially the upper right corner of the plates were still raised relative to the center of the plate, but the worst cases were only on the order of ~ ½". It should be noted that clamping the plates in this manner induces significant internal stresses; this may affect local sound speed, which may in turn contribute to inaccuracies in local amplitude and thickness measurements. Quantification of the effects of residual stress is the subject of an unfunded priority task under the Intelligent Integrated Machining work package.

Detecting unbonded regions with ultrasound is relatively straightforward using a through-transmission (TT) method. When TT is not feasible (due to lack of equipment, single-sided access to the part, etc.), pulse-echo (P/E) ultrasound can be employed. Identification of delaminations with P/E relies upon detection of amplitude changes and/or phase reversals. Amplitude reflection coefficients for sound traversing an interface between materials of different impedance are readily calculated from standard equations. In this application, however, because the HIPped plates are not really flat the transducer may not be precisely normal to the surface at all points and therefore the reflected signal recorded by the transducer may include additional unexpected geometric distortions; thus amplitude alone may not be a reliable indicator of an unbonded area, particularly if the plate is under additional stress from clamping. Fortunately, overall reflection polarity is less likely to be negatively impacted by small transducer/surface misalignments. When sound passes from a low impedance material such as Al into a higher impedance material such as DU-10Mo, the reflection polarity remains the same provided there is a good bond between the two materials. If instead the sound encounters a delamination, the reflection polarity is reversed and a multiple of the front surface is typically seen at twice the timing distance. This concept is illustrated in Figure 9.

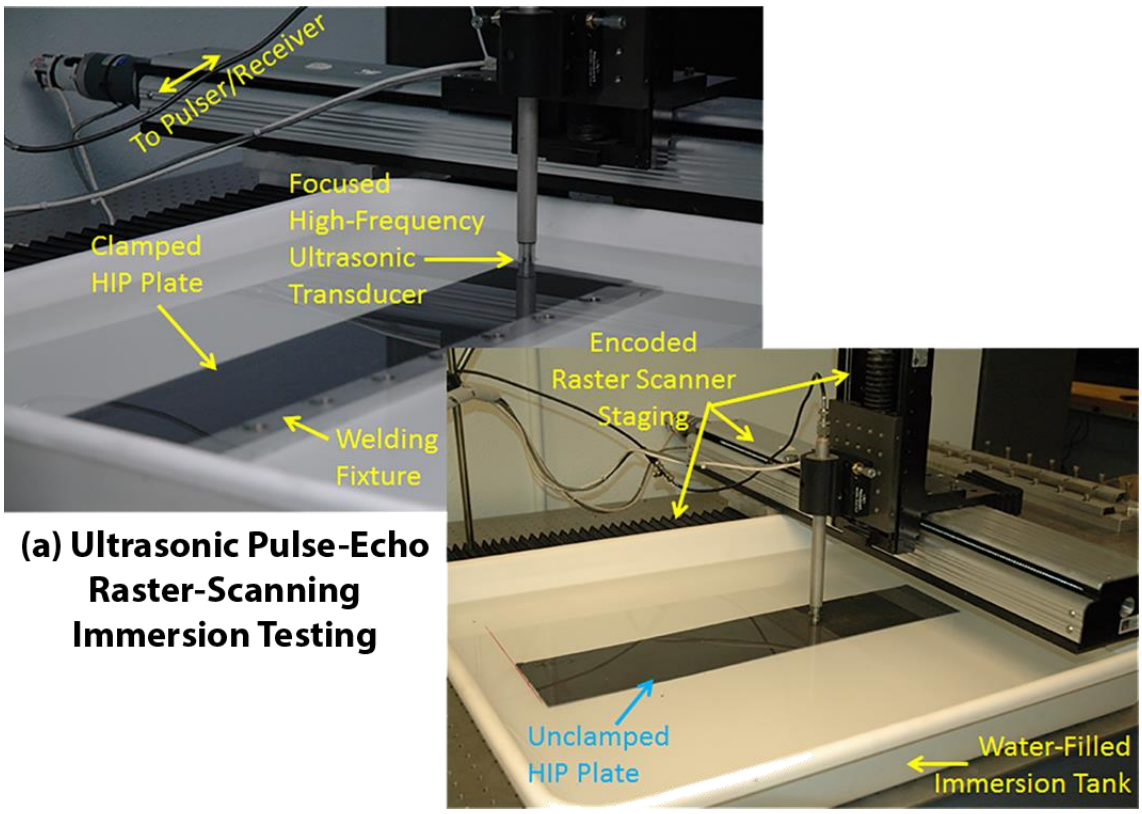

(a) Ultrasonic Pulse-Echo Raster-Scanning Immersion Testing

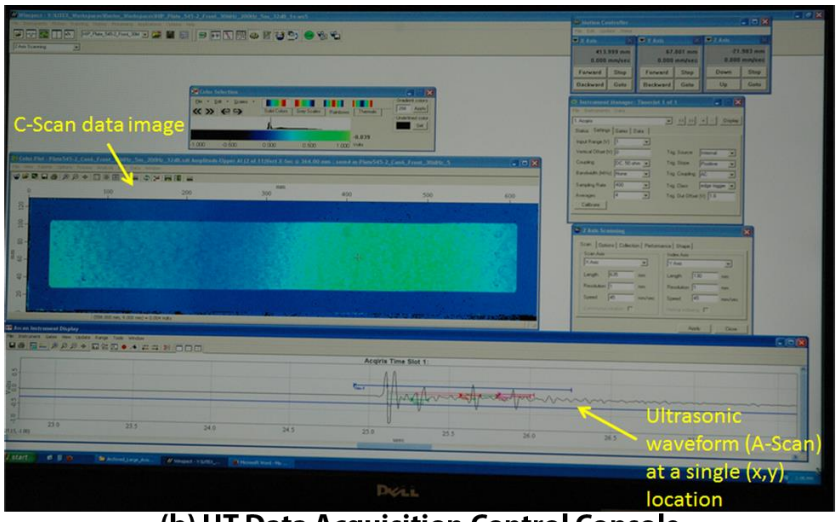

(b) UT Data Acquisition Control Console

Figure 8: Ultrasonic scanning set-up for pulse-echo immersion testing of HIPped fuel plates. (a) Tank, staging, transducer, clamped and unclamped samples. (b) Computer control console showing real-time A-Scan waveform data and C-Scan amplitude image.

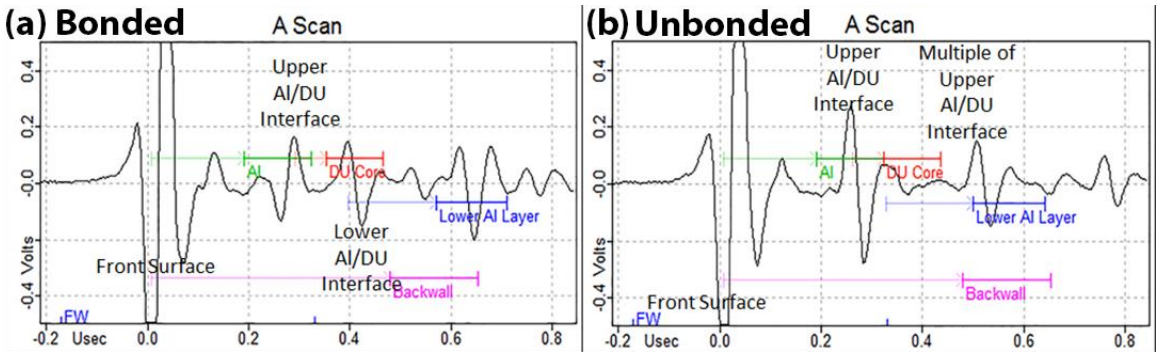

Figure 9: Ultrasonic waveform polarity seen in HIP plate inspection. (a) In bonded regions, as sound traverses from the front surface across the first Cladding/Core interface (green gate) it retains the same polarity as the initial (front surface) signal. Sound reflecting off the lower core/cladding interface (red gate) shows similar amplitude and reversed polarity from the signal at the previous interface. The lower core/cladding interface is located at a timing distance equal to the thickness of the fuel core material. (b) In an unbonded region, the polarity of the signal at the upper cladding/core interface (green gate) has the opposite polarity as compared with the initial (front surface) signal (or as compared with the same signal in the well-bonded region seen in (a)). No identifiable peak is seen at the expected location of the lower core/cladding interface; rather, a multiple of the upper cladding layer is seen at a timing distance equal to twice the cladding thickness.

To determine thickness, an ultrasonic time of flight (TOF) measurement is made between successive peaks representing the front and back interfaces of the layer in question. Thickness is calculated using the material sound speed for the layer, which must be correctly calibrated to ensure accurate results. Generally speaking, the wavelength of the sound in the material—determined by the transducer center frequency and material density and elasticity—must be no greater than the thinnest layer to be measured. Details of the TOF thickness measurement and thickness calculation are given in Figure 10.

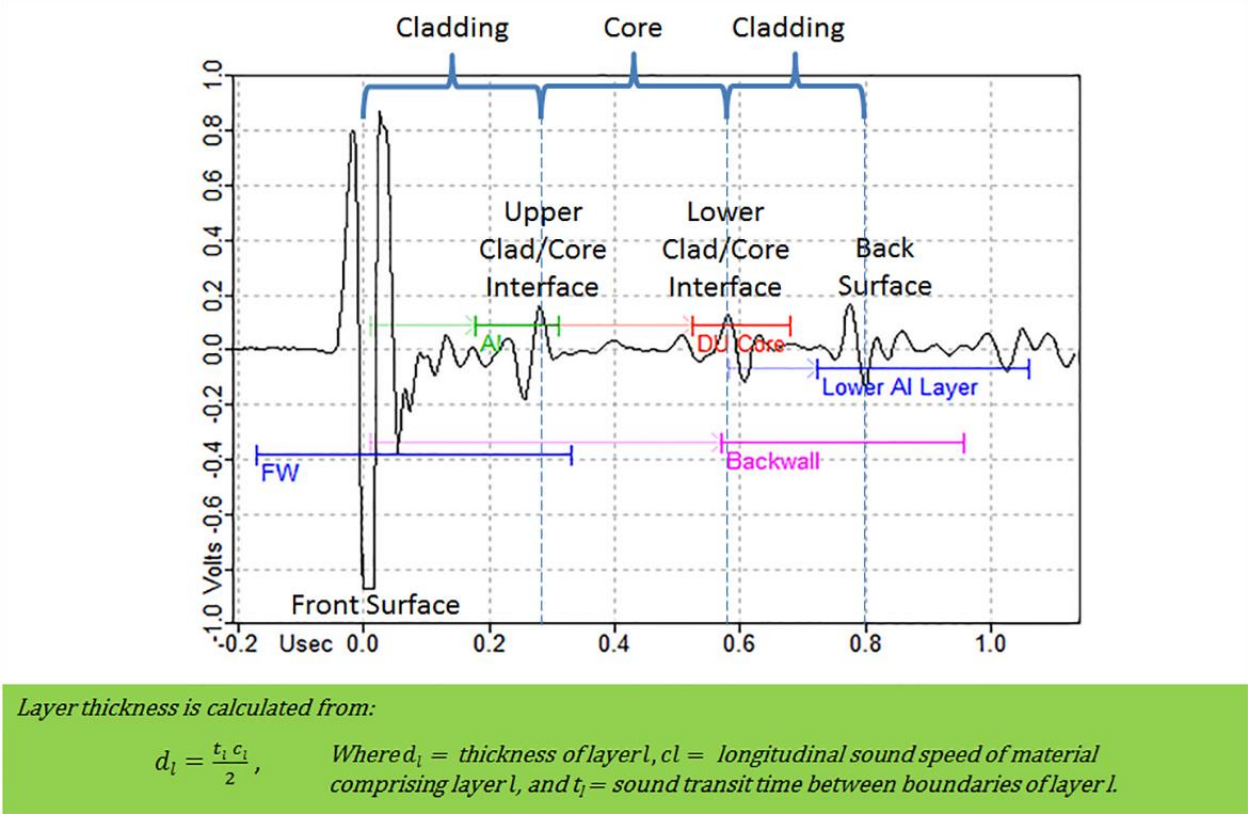

Layer thickness is calculated from:

$$d_l = \frac{t_l\, c_l}{2}, \qquad \textit{Where } d_l = \textit{thickness of layer } l, cl = \textit{longitudinal sound speed of material comprising layer } l, \textit{ and } t_l = \textit{sound transit time between boundaries of layer } l.$$

Figure 10: Thickness measurement via ultrasonic time-of-flight (TOF). In this application, compressional/longitudinal waves are assumed. Sound velocity for HIPped Al-6061 was calibrated by making UT round-trip transit time measurements at distinct locations along the edges of a sample plate and using caliper-based thickness measurements to back out the sound speed. The sound speed for HIPped Al-6061plates used in these experiments was determined to be 0.259 in/μsec, which is slightly faster than the literature values for generic aluminum. A sound speed value of 0.142 in/μsec for DU-10Mo was derived by applying a mixture law to the literature values for U and Mo.

As noted earlier, at a minimum all plates were scanned from the front surface; some plates were rescanned from the back surface as well. In all cases, 1.0 – 1.2 μsec of full waveform data was collected using a floating gate triggered off the front surface of the part. Data was re-gated offline to create amplitude, phase and thickness images of the individual cladding and core interfaces and layers. In this preliminary analysis, no additional post-processing has yet been performed. Note that the Zr co-rolled layer is too thin to be isolated as a separate layer at this time; additional analysis/experimental correlation is necessary to determine exactly how the Zr effects the various TOF thickness calculations. Quantitative observations for the 24 plates tested are compiled in Table 3; images for specific plates with findings of interest also follow.

Table 3: Ultrasonic Test Results (Initial Qualitative Observations)

HIP Can	Plate ID	Thick/Thin?	Nominal thickness	Length (mm)	Width (mm)	Comments
1	525-1	Thin	0.009"	578	76	Erroneously marked as 548-1. Unbonded elliptical region measuring 23 x 53 mm at the front interface. The unbonded region starts at he upper edge of the foil approximately 60 mm in from the left edge of the foil.
	540-1	Thick	0.022"	578	76	Erroneously marked as 529-1. Small region of questionable bonding status over the upper right corner of the foil. Two small oval regions of the lower cladding layer exhibit slight thinning towards the bottom right-hand side (when viewed from the front surface of the plate). The upper Al cladding exhibts very slight thinning in a triangular shaped region over the right edge of the foil and extending the entire width of the foil.
	548-1	Thick	0.022"	580	75	Erroneously marked as 525-1. Appears well-bonded over entire foil. A small circular disbonded region is noted in the Al-Al region in the lower right-hand edge.
	529-1	Thin	0.009"			Erroneously marked as 540-1. No bonding anomolies noted. Four apparent low-spots in the lower Al cladding.
2	527-1	Supposed to be thin, but really thick		578	76	Well bonded. Area of thinned Al seen in the upper central portion of the lower clad layer. (Really foil 548-2?)
	530-1	Thin	0.009"	579	75	Well bonded, uniform cladding layers.
	548-2	Supposed ot be thick, but really thin		579	76	Well bonded over foil. Several slighly thinned regions in upper cladding noted. (Really foil 527-1?)
	549-1	Thick	0.022"	578	75	Rear cladding appears well-bonded. Front cladding exhibts a large rectangular region of high amplitude extending 150 mm in from the right edge of the foil and approximately 2/3s of the way down the foil from the top edge. This region is most likely unbonded, or at best poorly bonded.
3	531-1	Supposed to be thin, but really thick		579	76	Well bonded over foil. Small triangular area of thinned cladding in lower clad layer over upper left edge of foil (as viewed formt he front surface). Upper cladding appears fairly uniform. Right edge of foil appears slightly short of the edge of the pocket, lower right edge is possisbly just outside the pocket. (Really foil 550-1?)
	549-2	Thick	0.022"	578	75	Upper and lower interfaces exhbit no discernable bonding anomolies. Upper cladding appears fairly uniform, lower cladding exhibits a circular region of thinning towards the upper left about a quarter of the way in from the edge of the foil. There is an indication (crack?) measuring approximately 20 mm in length and extending up obliquely for approximately 5 mm in the center of the DU-10Mo. The indication starts at ~398 mm from the left edge and 18 mm from the bottom edge of the foil.
	533-1	Thin	0.009"	579	76	Bonding looks intact. Upper and lower Al cladding appears thicker all around the dges of the central foil. Aluminum at the outer edges of the plate is thicker than the inner edges (before one reaches the cedntral foil).
	550-1	Supposed to be thick, but really thin		576	76	Bonding appears intact. Upper Al cladding is uniform thickness, lower cladding shows one are just left of center that appears significantly thinned. This could be due to stress effects, as this area was subject to greatest str5ess when plate was flattened for scanning; suggest sectioningat this location for ground truth. (Really foil 531-1?)
4	527-2	Thin	0.009"	449	76	Bonding over foil appears intact. Right edge of outer Aluminum is not bonded. Slight thinning over edges of foil in upper cladding, one small circular regoin of thinning in lower cladding; could be stress-induced.
	543-1	Thick	0.022"	580	74	Overall bonding appears good. Some thinning noted in both upper and lower cladding over the right-hand side of foil.
	543-2	Thick	0.022"	579	75	Significant speckle in data would suggest multiple small disbonded areas on both interfaces, particularly in the upper right of the top-most cladding layer, although examination of the B-scan data suggests some kind of internal defect throughout the upper aluminum cladding with particular issue in the upper right region.
	528-1	Thin	0.009"	504	74	Bonding appears intact, both layers of Al cladding appear fairly uniform.
5	528-2	Thin	0.009"	446	76	Bonding appears intact at both interfaces. Slight areas of non-uniformity in both cladding layers.
	542-1	Thick	0.022"	580	75	Some speckle seen in upper and lower phase images, appears to be surface related. Slight thinning seen in the upper left and lower right cladding layers.
	531-2	Thin	0.009"	436	77	Bonding appears intact. Lower cladding appears very uniform. Significant speckle in upper cladding thickness image. B-Scan data suggests some kind of internal defect within the upper Al layer itself.
	544-1	Thick	0.022"	581	74	Bonding appears intact. Slight thinning noted in on the right side for both the upper and lower cladding layers.
6	532-2	Thin	0.009"	439	76	Upper interface bonding intact;, lower interface contains some speckle on left side along edge of foil and upper right corner of foil, likley false indications judging from full waveform data.
	545-1	Thick	0.022"	579	77	Bonding intact, cladding fairly uniform.
	533-2	Thin	0.009"	439	74	Bonding over foil appears intact. The aluminum is either not bonded to itself at the very right hand edge of the plate. The upper cladding layer data shows a lot of speckle, appears to be related to surface bubbkles on the part. The lower cladding shows very slight thinning asa one moves from the center towards the edges of the foil.
	545-2	Thick	0.002"	582	75	Significant speckle in both phase images, but on B-scan bonding appears intact. Thinning of the upper cladding noted over the left edge and the right third of the foil. Lower cladding is slightly thinner over the right half of the foil.

As noted in the data table, bonding for most plates appears intact. One notable exception is Plate 525-1, one of the thin core samples from HIP Can 1. This can had what appeared to be a raised area on the front surface over the left edge of the fuel foil. UT phase images from the front and back of the plate (Figure 11) show a roughly 1" x 2" unbonded region at the front cladding/core interface. Whether this delamination exists between the Al and the Zr or the Zr and the DU-10Mo is undetermined. Time-of-flight and horizontal B-Scan images of the same plate (viewed from the front) are shown in Figure 12.

(a) Plate 525-1: Viewed from Front

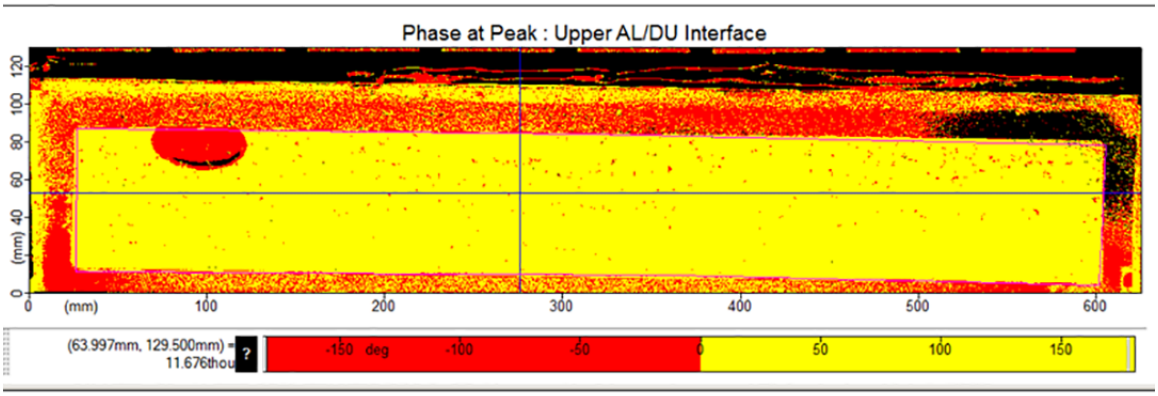

(b) Plate 525-1: Viewed from Back

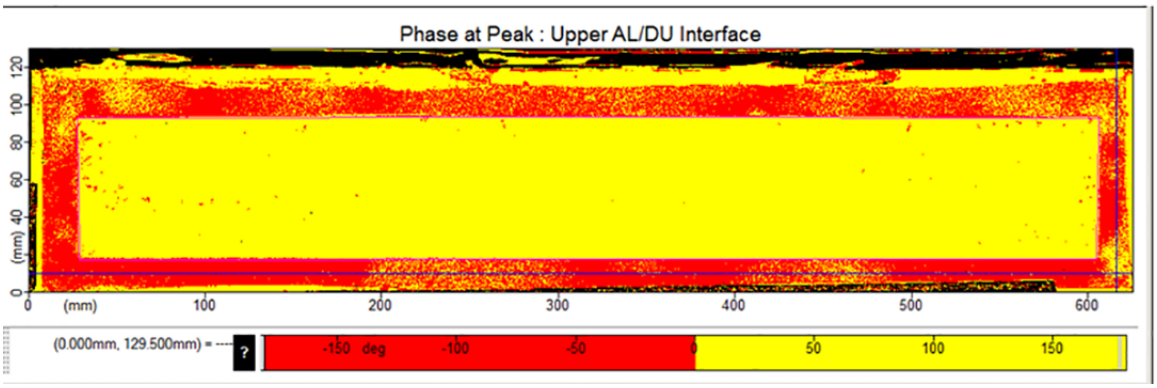

Figure 11: Ultrasonic phase images for Plate 525-1 (HIP Can 1). Data is gated to reflect true phase over the central fuel foil. In the aforementioned region, bonded regions are yellow and unbonded regions are red. (a) Upper core/cladding interface as viewed from the front of the plate. An unbonded 23 x 53 mm elliptical-shaped area is noted over the upper left edge of the fuel foil. (b) Phase image of the first core/cladding interface encountered when viewed from the back (corresponding to the lower core/cladding interface when viewed from the front). This interface appears completely bonded.

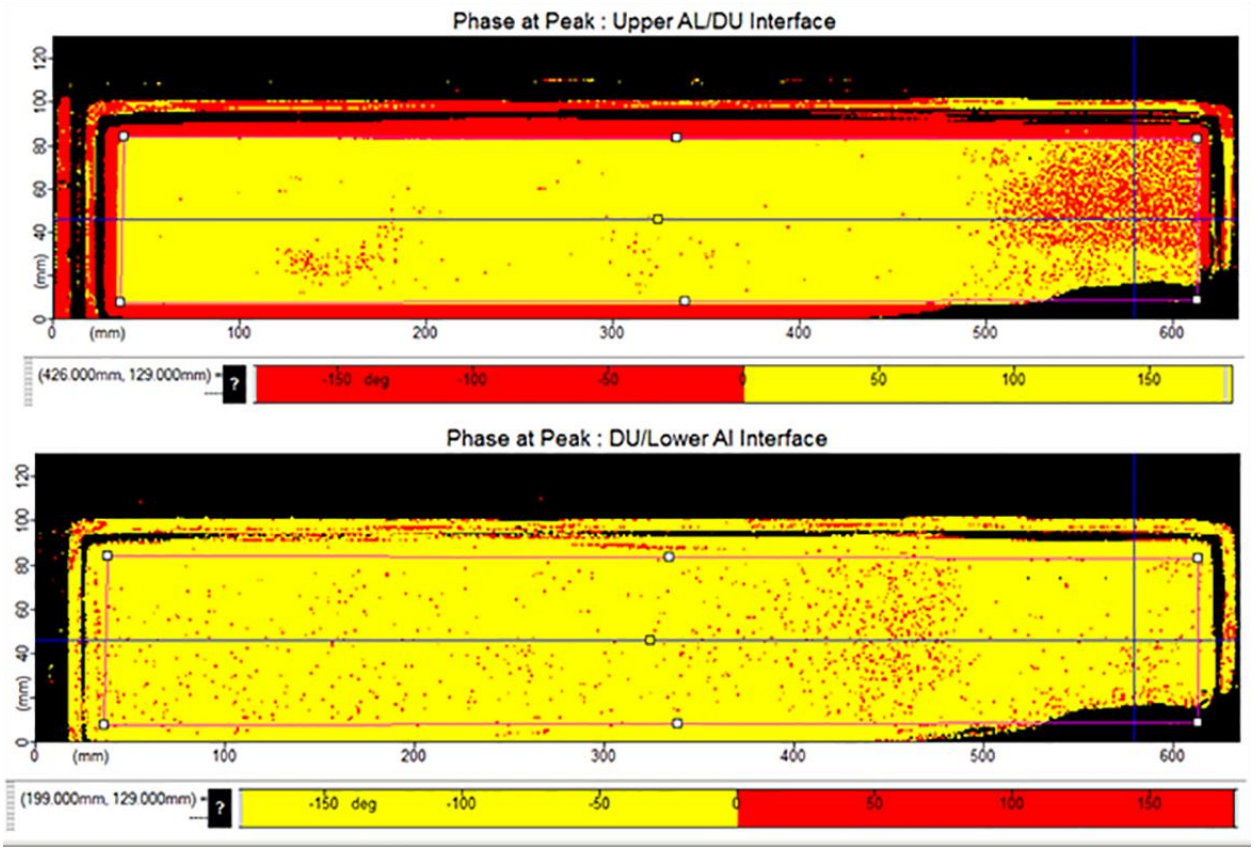

Figure 12: Ultrasonic B-Scan and Time-of-Flight images for Plate 525-1 (HIP Can 1). (a) The B-Scan image shows a cross-sectional image of the plate at a given horizontal location. The position along the length of the plate maps to the x-axis, while time, which is equivalent to distance into the plate, is on the Y-axis. The front surface of the plate is represented by the solid yellow/black/white line towards the top of the y-axis running across the width of the plot. Interface echoes and their interpretations are noted on the image. (b) Time-of-flight thickness image of the upper surface of the plate, showing a large anomaly over the upper left edge of the fuel foil. Gating is such that thickness calculations are only valid over the bonded regions of the cladding over the central fuel foil (interior of pink rectangle).

A fairly large anomaly, most likely a sporadically unbonded area, is identified at the upper core/cladding interface in Plate 549-1 (Can 2), as shown in the phase images in Figure 13. In addition, significant speckle is seen throughout the upper and lower interface phase images, but upon examination of the B-Scan data (Figure 14) these regions appear to be intact. There is an extremely high amplitude backwall signal seen in the aforementioned rectangular region at the right end of the foil, as seen in Figure 14, which reinforces the interpretation of a delamination, or at least something unusual, in this region of the plate.

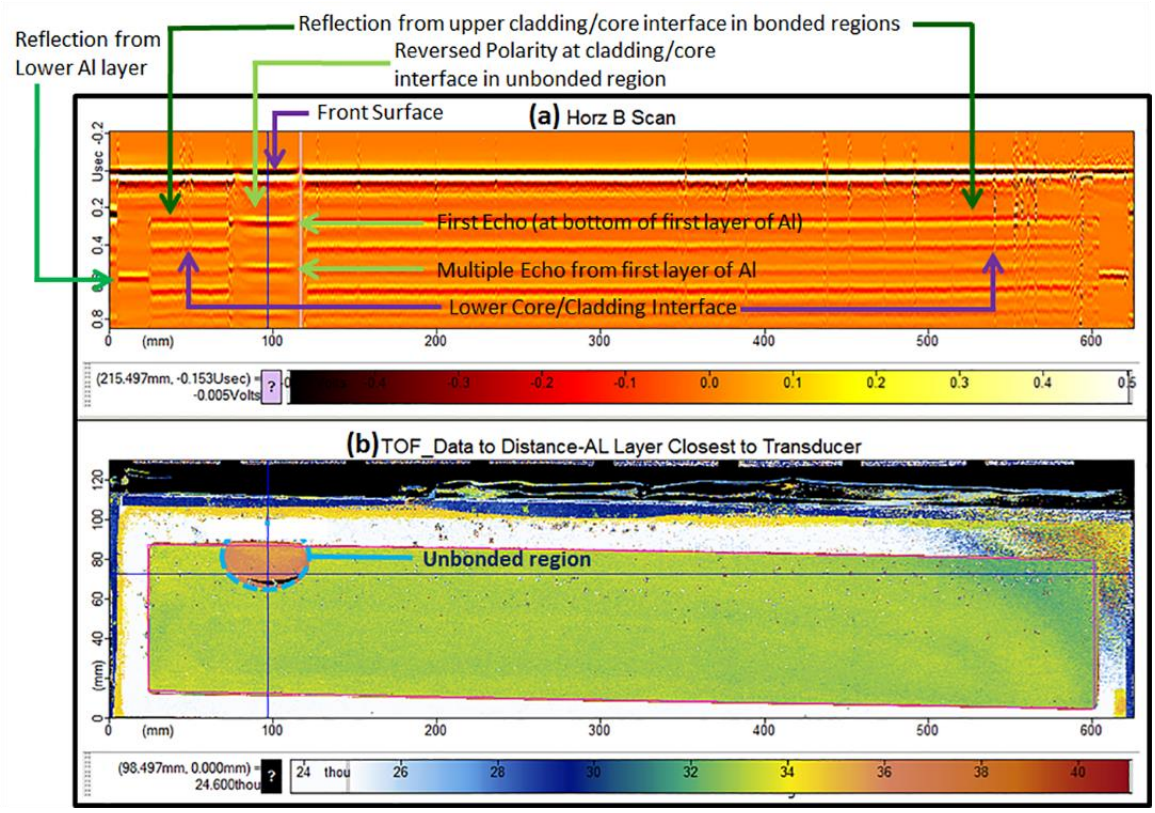

Figure 13: Phase images for the upper and lower core/cladding interfaces in Plate 549-1 (Can 2), showing a large rectangular anomaly over the right section of the foil at the upper interface.

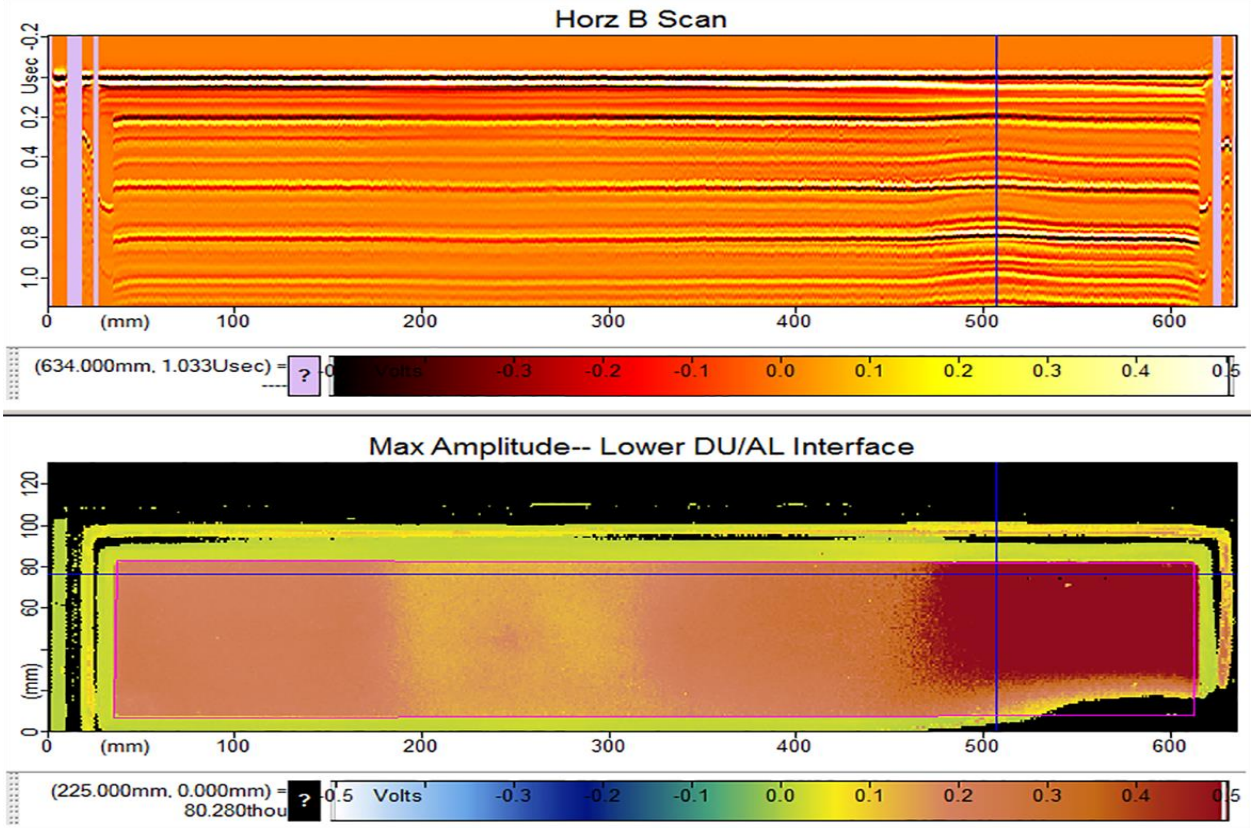

Figure 14: B-Scan and amplitude images for plate 549-1 (Can 2) showing large anomalous, likely unbonded, region at the right edge of the foil insert.

Plate 549-2 (Can 3) was interesting for several reasons. Phase images for this plate indicate intact bonding for both the upper and lower interfaces (Figure 15). The TOF thickness images show a very uniform upper cladding layer (Figure 16), and a lower cladding layer that is fairly uniform with the exception of a roughly 40 mm diameter circular region that is up to 0.003" thinner than the surrounding cladding (Figure 17). The minimum cladding thickness (minclad) in this region is measured at 26.3 mm. One surprising finding, noted only incidentally when scrutinizing the full waveform data more closely, is an apparent crack in the DU-10Mo fuel core, as seen in Figure 18. The lower left edge of this indication is located at 415 mm in from the left rim and 84 mm down from the upper rim of the plate (Al edge); the indication measures approximately 20 mm in length and is oriented obliquely in 3 dimensions. The top of the indication first appears at 0.347 μsec, or 0.0064" from the top of the fuel insert, and extends to

0.470 µsec or 0.0151” from the upper fuel surface.

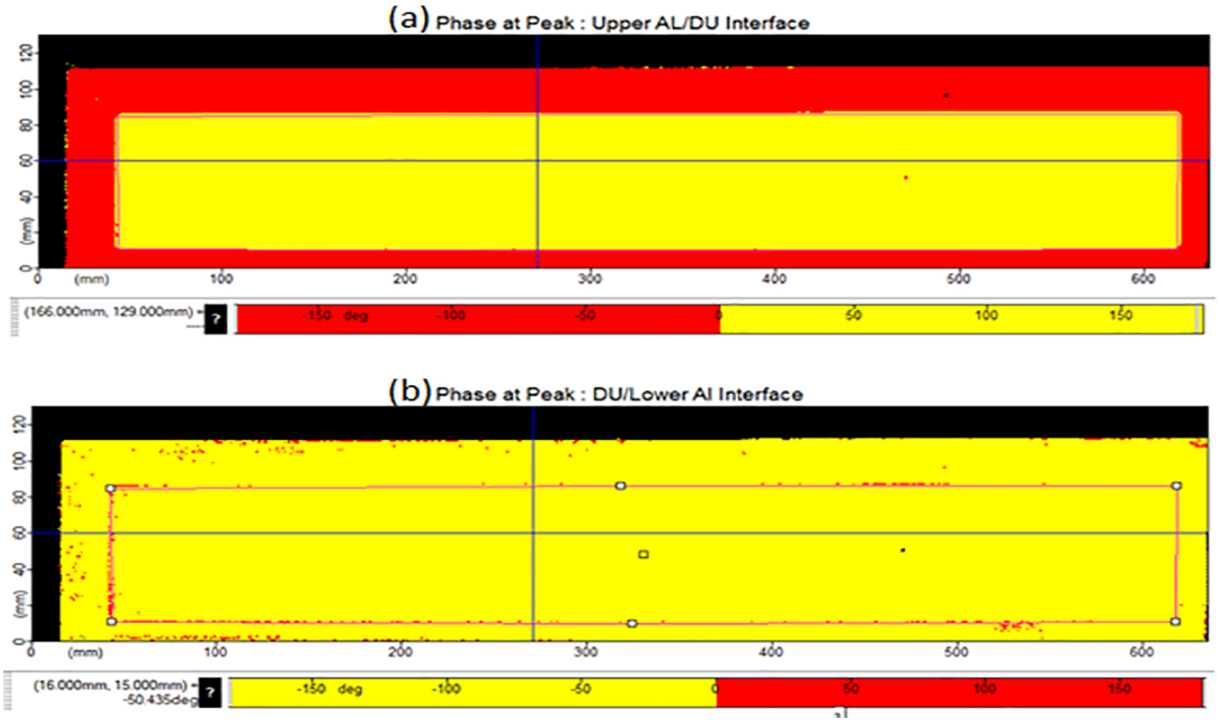

Figure 15: Plate 549-2 (Can 3) phase images showing intact bonding over the upper and lower core/cladding interfaces.

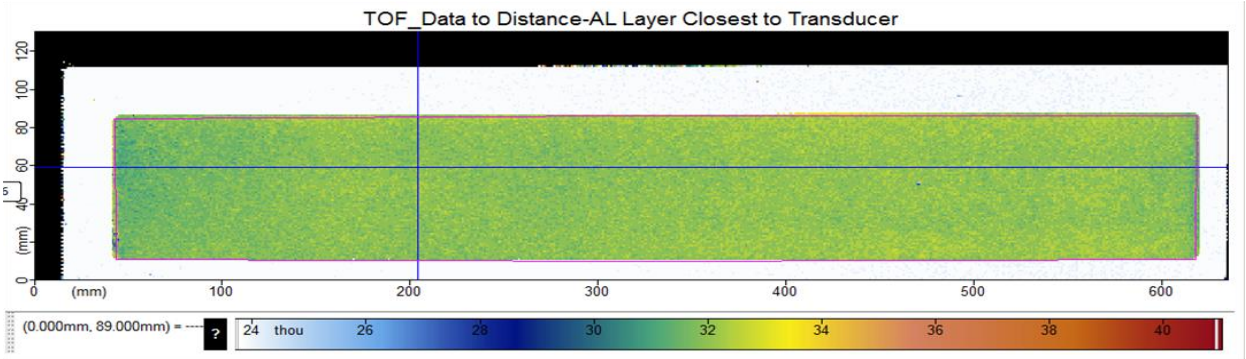

Figure 16: Plate 549-2 (Can 3) TOF distance image showing uniform upper cladding thickness.

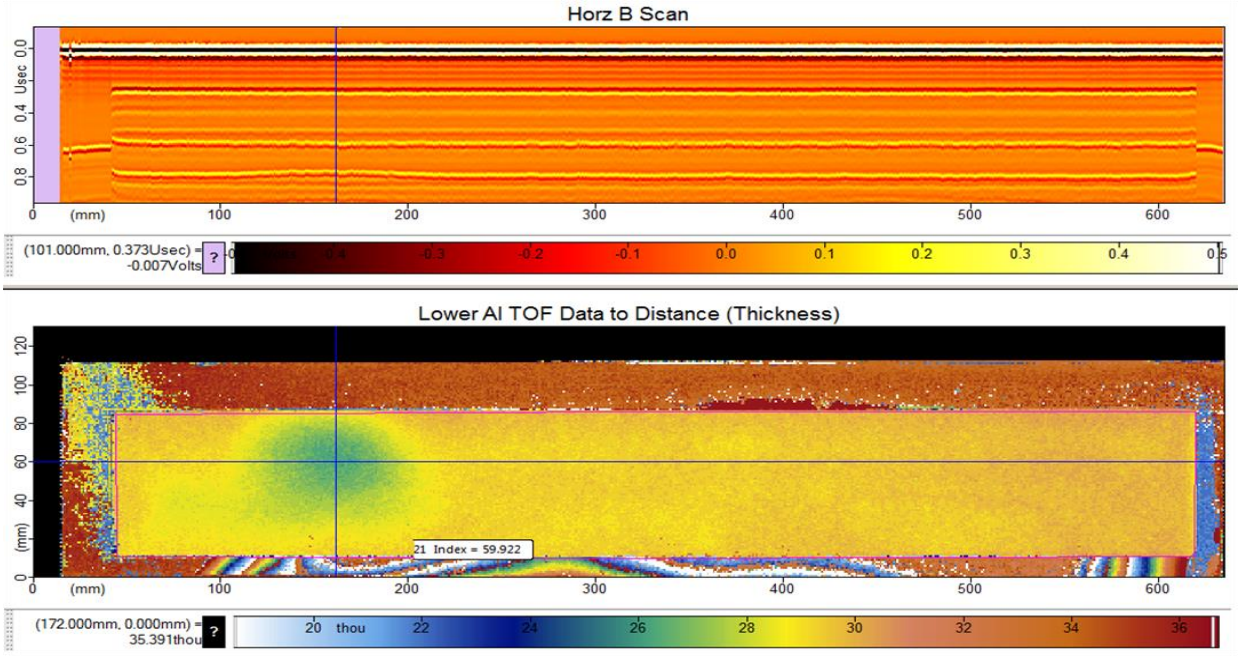

Figure 17: Plate 549-2 (Can 3) TOF distance image showing a relatively uniform lower cladding thickness punctuated by a 40 mm diameter thinned region (green area) measuring up to 0.003" thinner than the surrounding material (minclad 26.3 mm).

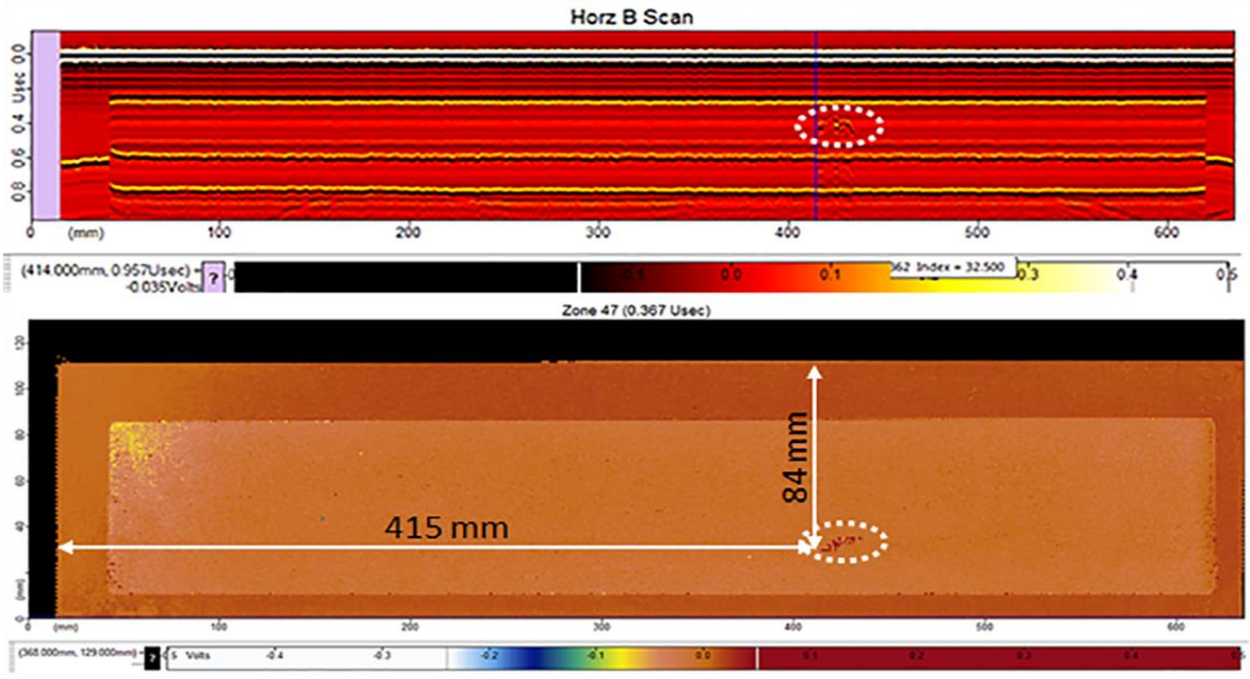

Figure 18: Plate 549-2 (Can 3) B-Scan waveform image (top) and C-Scan image at a single point in time corresponding to a single depth within the plate (bottom). An oblique crack-like indication roughly 20 mm in length is identified (dotted oval). The indication extends through contiguous depth slices ranging from 0.0064" to 0.0151" from the upper surface of the fuel core.

As shown in Figure 16, an area of Al-Al disbonding is seen in Plate 527-1 (Can 4). The unbonded region manifests itself as an area of higher amplitude reflection in the backwall amplitude image, and a reflection at the Al-Al interface in the waveform images (A & B-scans).

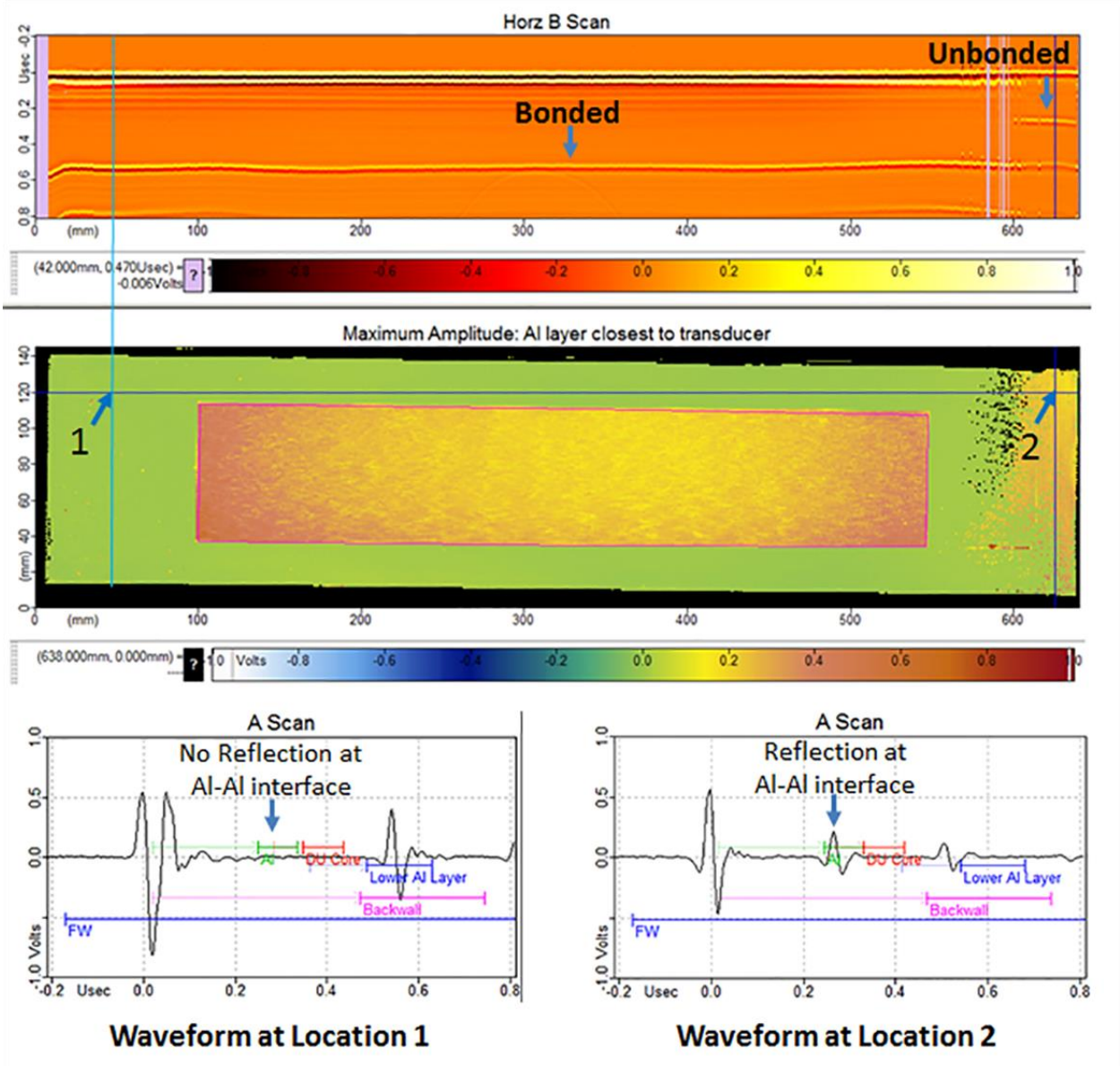

Figure 16: B-Scan, Amplitude, and A-Scan waveform images for Plate 527-1 (Can 4) showing an unbonded region at the right edge of the plate. A reflection at the Al-Al bondline is apparent in the unbonded case (location 2). No such reflection is seen in areas where the Al-Al bond is intact (e.g., location 1).

In summary, preliminary pulse-echo UT results based on the raw, unprocessed data indicate good bonding over most of the HIPped plates, with the exceptions of those noted. Qualitative results indicate some variation in the overall cladding thickness; a more thorough analysis and

metallurgical correlation is required to calibrate in absolute numbers and to distinguish/account for Zr thickness and effects of residual stress and geometric distortions in the overall thickness measurement.

Infrared thermography is a potential alternative to UT inspection for bond assessment; this would be an extremely fast measurement (several seconds vs 30 minutes/plate), however it may suffer from similar issues with regard to sample flatness and residual stress effects. In-house tests with existing equipment were unsuccessful due to a) insufficient vacuum within the cryo-cooling system (a maintenance issue) and b) a lens that was not optimally matched for the intended measurement. Newer commercially-available IR cameras, particularly those that incorporate Thermal Wave Imaging's patented Thermographic Signal Reconstruction *(*TSR*)* technology, appear well-suited to the HIPped plate bonding assessment application.

2.5 Samples for Metallography

At least one plate from each of seven HIP cans was designated for metallography, microhardness, and mechanical bonding (MMM) measurements to evaluate the integrity of the Al-Al bond and Al-Zr bond, and evaluate any variations/deviations as a result of the HIP process. This plate will be designated as "MMM" plate. Samples for metallography and potential microhardness and mechanical bonding were sectioned from the MMM plates at a minimum of five locations (including both ends of the plate and the center). Figure 17 shows the identification numbers (IDs) and locations of each samples. Full size plate is 25" long by 5" wide; foil within is 23" long by 3" wide. Center of the plate is the rightmost boundary of areas marked 16, 17, 18. One quarter distance is the rightmost boundary of areas marked 10, 11,12. Samples for optical microscopy, SEM, and microcantilevers are 1 - 3; 10 -12 and 16 - 18. Samples for bulge testing are 7, 8, and 14. Spare samples for further microscopy or alternative bond strength testing are 4, 6, 7, 9, 13 and 15.

<table>
<tr><td>3</td><td>6</td><td rowspan="3">19</td><td>9</td><td>12</td><td rowspan="3">20</td><td>15</td><td>18</td><td rowspan="3">21</td></tr>
<tr><td>2</td><td>7</td><td>8</td><td>11</td><td>14</td><td>17</td></tr>
<tr><td>1</td><td>4</td><td>7</td><td>10</td><td>13</td><td>16</td></tr>
</table>

Figure 17: The IDs and locations of each samples.

2.6 Bulge Test

Three (3) bulge specimens were machined from Al/Zr/DU-10wt%Mo plate (ID: 529-1). Figure 11 is a schematic showing the design of the bulge test. A circular disk, with 1" in diameter, was machined from the HIPed plate. On one side of the disk, a circular recess with diameter *D* was machined and the depth of this recess is such that it stops at the interface between Al and the Zr/DU-10wt%Mo, as shown in Figure 18(a). This circular disk is then glued to a stainless steel circular backing disk with 1" in diameter. This specimen assembly is positioned in a pressure cell and distilled water was injected into the recess using a syringe pump, so that hydraulic pressure

P is applied to the top Al foil, with the initial thickness of *h*, to deform it and generate a bulge. When the pressure is high enough, stress concentration at the corner of the recess will cause the delamination of the Al foil along the interface between Al and Zr/DU-10wt%Mo. 3D-DIC was used to measure the profile of the deforming bulge and the deformation field across the bulge surface. Figure 18(b) shows the sample IDs, thickness and diameter of each disc. Nominal recess diameter is $D = 0.375$" for all three discs.

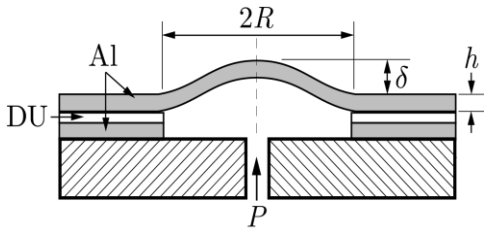

(a)

Sample No.	Thickness h (mm)	Diameter D (mm)
529-1-7	0.760	9.4777
529-1-8	0.777	9.4678
529-1-14	0.834	9.4777

(b)

Figure 18: (a) A schematic showing the design of the bulge test, (b) the sample IDs, thickness and diameter of each disc. Nominal recess diameter is $D = 0.375$" for all three discs.

For one of the Al/Zr/DU-10wt%Mo specimens, 529-1-08, the variation of applied pressure P as a function of the overall deflection of the deforming bulge δ is presented in Figure 19(a). Here the deflection δ is normalized by the initial thickness of the Al foil *h*. The profiles of the evolving bulge obtained by using 3D-DIC are shown in Figure 19(b). In the figure, the associated applied pressure *P* at each instant of time is also shown. The color in the plots represents the elevation of the bulge *w* at any given location, measured from the initial flat sample surface and normalized by the initial thickness of the aluminum foil *h*. As the applied pressure increases, the bulge enlarges continuously.

Figure 20 illustrates the scheme for identifying the bulge boundary or the location of the interfacial crack front. On the left of Figure 20, the contour plot of the minor principal strain ϵ_2 at the moment F indicated in Figure 19(a) is presented. For any polar angle θ, originating from the center of the bulge and measured from the x-axis, and along the radial direction r, the location of local minimum of ϵ_2 long that direction is determined numerically. This process is repeated for all $0 \leq \theta \leq 2\pi$ and the closed loop of the local minima of ϵ_2 is thus determined. This closed loop is shown in the contour plot for ϵ_2 as the dashed line. The same procedure is also applied to the mean curvature κ_{mean} field shown on the right of Figure 20, where the local maxima of κ_{mean} is identified for all $0 \leq \theta \leq 2\pi$, and the closed loop of such local maxima is shown in the contour plot for κ_{mean} as dashed line as well.

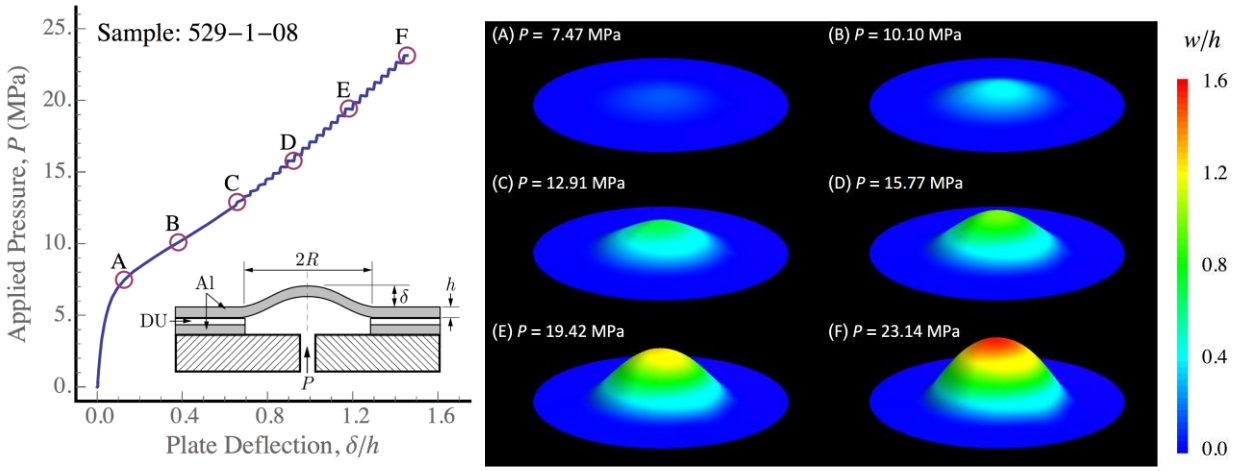

(a) (b)

Figure 19: (a) Overall response of the Al/Zr/DU-10wt%Mo specimen 529-1-08, (b) evolution of the bulge in the Al/Zr/DU-10wt%Mo specimen 529-1-08 at selected moments of time during the bulge test. The associated applied pressure at each instant of time is also shown.

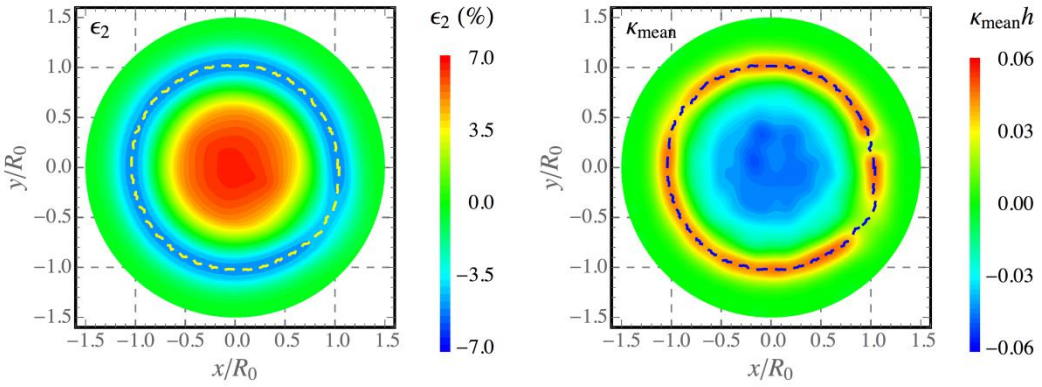

Figure 20: Contour plots of the minor principal strain ϵ_2 and the mean curvature κ_{mean}, together with the identified boundary of the bulge, of the Al/Zr/DU-10wt%Mo specimen 529-1-08 at the particular moment F.

Repeat this procedure for any given moment during the bulge test, the progression of the bulge boundary or the motion of the interfacial crack front can be determined. Figure 21 presents the bulge boundary of the test specimen 529-1-08 at three selected moments, D, E, and F as indicated in Figure 10(a). Detectable amount of delamination of the Al/Zr/DU-10wt%Mo interface is captured from the bulge boundaries shown in Figure 20.

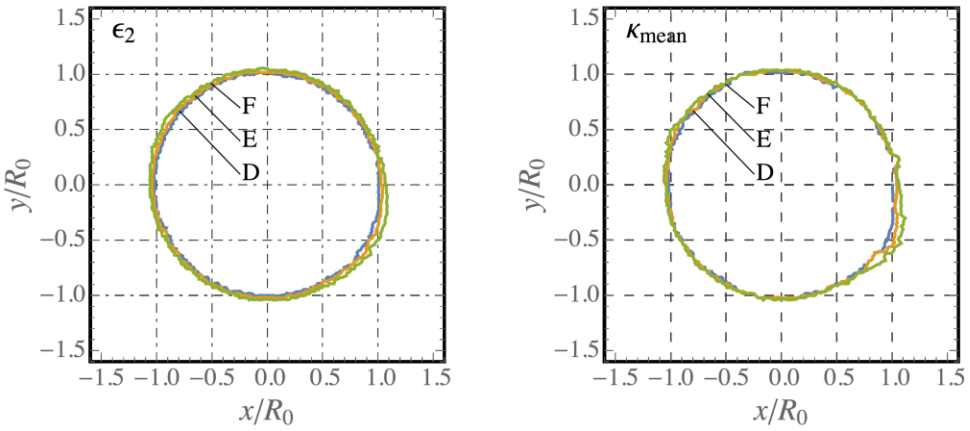

Figure 21: Bulge boundary determined by either the minor principal strain ϵ_2 or the mean curvature κ_{mean} at three selected moments, D, E, and F as indicated in Figure 19(a).

In fracture mechanics, the energy-release rate is defined as the energy dissipated during fracture per unit area of newly created material surface. The energy-release rate also characterizes the resistance of a material or an interface to fracture, since it identifies the amount of energy required for forming new surfaces inside the material or along the interface. In the bulge test, we are able to measure quantitatively the energy for creating new surface along the Al/Zr/DU-10wt%Mo interface, as indicated by the shaded area or the open symbols in Figure 22(a). In the meantime, we are able to determine the area of the newly formed surface due to delamination of the Al/Zr/DU-10wt%Mo interface, as shown in Figure 22. Figure 22(b) presents the variation of the energy release Π against the bulging area A for the specimen 529-1-08. From the data shown in Figure 22(b), we see that major portion of the data follow a straight line for $\Pi > 0$. The slope of this straight line, i.e., $(\partial\Pi/\partial A)/2$, thus defines the so-called energy-release rate and for specimen 529-1-08, the energy-release rate for the stable extension of the Al/Zr/DU-10wt%Mo interfacial crack can be calculated to be 6.2 mJ/mm^2.

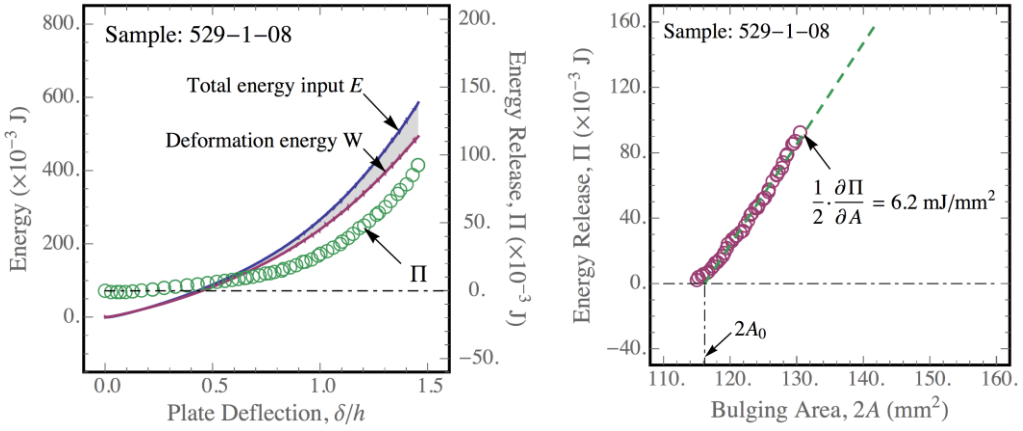

(a) (b)

Figure 22: (a) Energy partition during the miniature bulge test of the Al/Zr/DU-10wt%Mo specimen 529-1-08; (b) Variation of energy release Π, or delamination energy, as function of bulging area A for the Al/Zr/DU-10wt%Mo specimen 529-1-08. The slope $(\partial\Pi/\partial A)/2$ is the energy-release rate, or the fracture toughness.

Figure 23 presents the overall response of all three bulge specimens, where the applied hydraulic pressure P is plotted against the maximum deflection of the deforming bulge δ. The overall responses of the three specimens are quite similar. Also the maximum pressure (at moment F of each test) indicates that the interfacial strength of this Al/Zr/DU-10wt%Mo plate is relatively high compared to the other Al/Zr/DU-10wt%Mo plates we have tested so far.

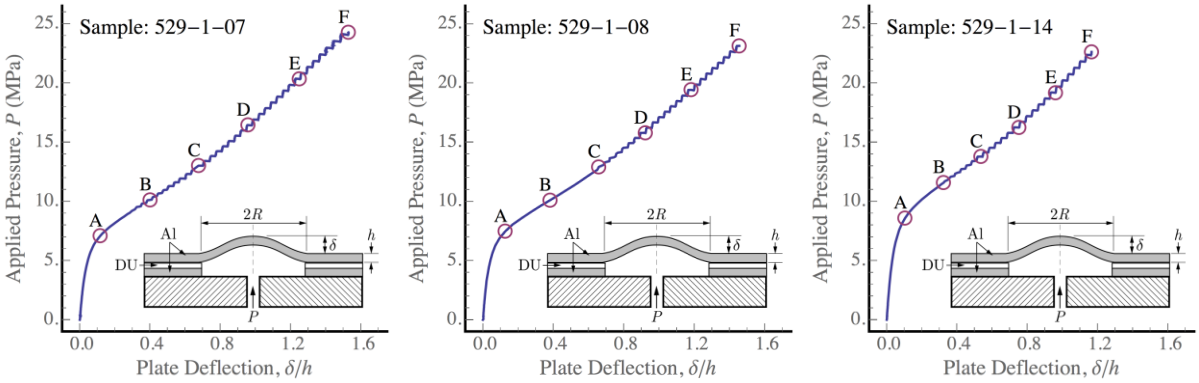

Figure 23: Overall responses of Al/Zr/DU-10wt%Mo specimens.

By carrying out the data processing procedures described above, the energy release rate, or interfacial fracture toughness, is determined for these three bulge test specimens. Figure 24 shows the plots of the energy release as a function of the delamination area, where the slope of the curve gives the fracture toughness. The fracture toughness results from the three bulge tests are consistent, although the measurement from specimen 529-1-14 is higher than the other two specimens. Overall the bulge test results indicate that the Al/Zr/DU-10wt%Mo plate we tested has a relatively high toughness.

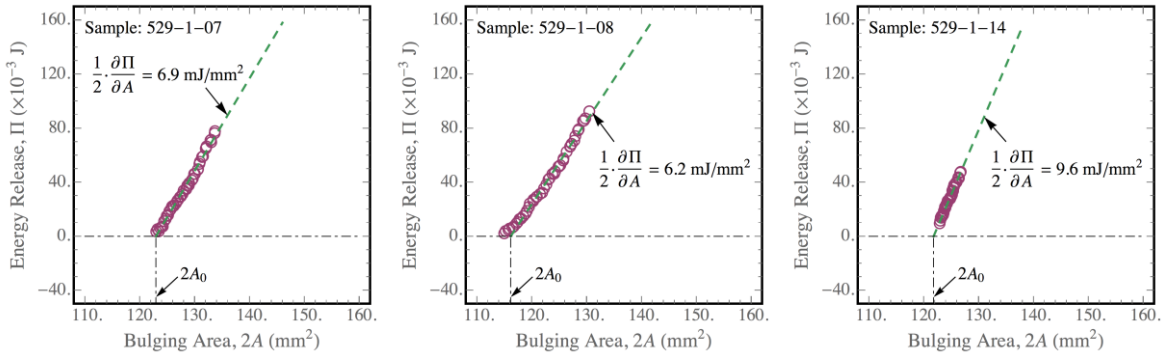

Figure 24: Variation of energy release Π, or delamination energy, as function of bulging area A for specimen of all Al/Zr/DU-10wt%Mo specimens.

2.8 Metallography Characterizations

Metallography was used to exam any microstructural anomalies in the plate, foil, and along the fuel-clad interface. The plate (ID: 540-1) with “fuzzy" data in ultrasound was selected for the metallographic examination. The goal was to know if the “fuzzy" data was noise caused by residual stress or real debonding. Figures 25(a), 25(b), and 25(c) are the optical micrographs showing the bonding of LEU-Zr, Zr-Al, and Al-Al. Figure 25(a) shows the typical bonding close to the end of the plate. From this micrograph, one can easily see that the bonding between LEU-Zr, Zr-Al, and Al-Al are well bonded without any crack, defect, or delamination. The interfaces are nice and clean without any distortion or pit, which results in a nice and flat LEU foil. Figure 25(b) is a view from the middle section of the plate. Again, the bonding between LEU-Zr, Zr-Al, and Al-Al are well bonded without any crack, defect, or delamination, which confirms that the whole plate has a consistence bonding from one end to the other. Figure 25(c) is a higher magnification showing the bonding of figure 1(a). The higher magnification shows the thickness of the zirconium cladding as well as the clear well bonding between LeU-Zr and Zr-Al. Also, the Al-Al bond line can be seen from the left hand bottom corner of the micrograph. The Al-Al bonding has a well bonded interface showing a nice and smooth interface without any unbonded interface or any delamination. Metallography has demonstrated that no debonding in these fuzzy area from the ultrasonic testing, therefore the conclusion is that residual stress was the reason for the “fuzzy” data.

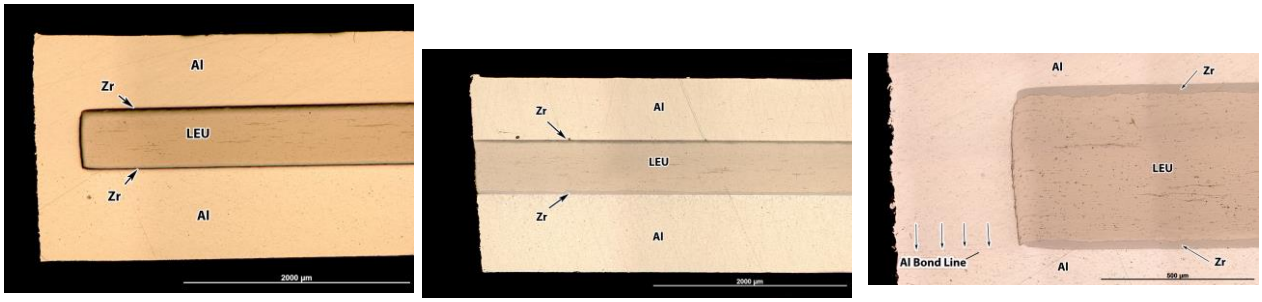

Figure 25: The optical micrographs showing the bonding of LEU-Zr, Zr-Al, and Al-Al. (a) the typical bonding close to the end of the plate, (b) a view from the middle section of the plate, and (c) a higher magnification showing the bonding of figure 1(a).

2.9 Foils for Rolling

A total of twenty-one plates were transferred to the rolling project. The plate IDs and thickness of the LEU foil and lengths are listed as follows.

From HIPCAN1-4FLS:

Plate# Thickness Length

525-1	0.009”	23"

From HIPCAN2-4FLS:

Plate#	Thickness	Length
527-1	0.009”	23”
530-1	0.009”	23"
548-2	0.022”	23”
549-1	0.022”	23”

From HIPCAN3-4FLS:

Plate#	Thickness	Length
531-1	0.009”	23”
549-2	0.022”	23"
533-1	0.009”	23”
550-1	0.022”	23”

From HIPCAN4-4FLS:

Plate#	Thickness	Length
527-2	0.009”	17.75”
543-1	0.022”	23"
543-2	0.022”	23"
528-1	0.009”	20”

From HIPCAN5-4FLS:

Plate#	Thickness	Length
528-2	0.009”	17.75”
542-1	0.022”	23"
531-2	0.009”	17.6”
544-1	0.022”	23”

From HIPCAN6-4FLS:

Plate#	Thickness	Length
532-2	0.009”	20.9”
545-1	0.022”	23"
533-2	0.009”	17.4”
545-2	0.022”	23”

2.10 Remaining Plates

The remainder of the plates were prepared as necessary for machining to one of two final dimensions in WBS 1.2.1.6. Each foil thickness will have representatives of each final cladding thickness: three plates will have 0.009 in. foil with 0.020 in. plate thickness (0.006 in. cladding on each side of foil), three plates will have 0.009 in. foil with 0.038 in. plate thickness (0.015 in. cladding on each side of foil), three plates will have 0.022 in. foil with 0.042 in. plate thickness (0.006 in. cladding on each side of foil), three plates will have 0.022 in. foil with 0.062 in. plate thickness (0.020 inch cladding on each side of foil), Finishing was by gang milling and utilized in-situ measurements of minimum cladding thickness by a handheld ultrasonic testing unit and a handheld x-ray fluorescence unit or a dedicated in-situ station if available. It should be noted that there is a cross over in relative accuracy of the two techniques at about 0.030 in. aluminum cladding thickness. UT is more accurate above 0.030 in. and XRF is more accurate below. Keyence laser measurements of surface finish and thickness was performed on all 12 plates.

This activity was completed in order to provide plates for plate forming experiments (WBS 1.2.1.6). This activity is a predecessor activity for all subsequent HIP bonding operations for demonstration related projects in the program, meaning that the baseline HIP bonding technique must be defined prior to demonstration of the fuel fabrication process. Fabrication of demonstration products drives a number of Level 0 and 1 Program Milestones. However, completion of this activity most directly affects the **Level 1 Milestone - BFD Fuel Fabrication Complete**. Thus, completion of this activity, although further upstream, contributes to the direct achievement of this milestone. Further, any refinements to the fuel fabrication process are futile without a solid understanding of a "baseline" process, which this activity aids to define.

3.0 Summary

LANL has successfully completed the HIP bonding process baseline demonstration work package. A total of 6 HIP cans with 24 plates were HIPped. The stainless steel HIP can had been designed using lessons learned from INL, LANL and B&W. Each HIP can was filled with an assembly consisting of DU-10Mo foils, strongbacks and a parting agent. All strongbacks and aluminum cladding are straight and flat. Total thickness of each aluminum cladding and foil set was 0.70 in. The interior of the HIP can and all metallic components are cleaned using a standard procedure qualified by surface science measurements, especially angle resolved photoelectron spectroscopy. The cleaning processes were developed in the LANL MST-6 Sigma Cleaning Facility. Within the scope of cleaning processes readily implemented or already available in the facility, new methods were developed for cleaning the various materials surfaces in this program, particularly for those materials and surfaces going into a bonding operation where cleanliness is paramount in forming a strong coherent interfacial bond. These cleaning processes were designed to be as efficient and effective as possible for the large area foils required for this program. The HIP can transported to an inert atmosphere glovebox where the final side was welded on under nitrogen atmosphere followed by degas the HIP can at 350^{o}C for ninety minutes. The HIP can was transported to a HIP. HIP tool place at 560^{o}C and 15,000 psi for 120 minutes. A total of twenty-one plates were transferred to the rolling project.

A finite element simulation of the HIP cycle was performed on the can assembly. Abaqus 6.14 Standard was used to simulate the 2D plane strain section of the HIP can assembly with half-symmetry. To accurately simulate the HIP cycles, an average of ten successful experimental HIP runs were used as the input conditions for temperature and pressure of the FEA. An elasto-platic temperature-dependent material model was used in the fully coupled transient temperature displacement analysis was used to simulate the hot isostatic pressing process. The Von Mises stress contour plot after the HIP process shows that higher stress concentration is found at the corners between the side plate and the top and bottom plate. This region is where the top and bottom plate plastically deforms filling the gaps inside the can. An even higher stress concentration area is found on the outer fuel plate assemblies, specifically where the aluminum cladding seals the U-10Mo fuel foil. The other two fuel assemblies located near the midpoint of the can do not show any high stress concentration. The highest amount of plastic deformation is located in the aluminum cladding which surrounds the U-10Mo fuel foils giving a sealed fuel foil assembly. The FEA simulation predicts increased thickness in the joint between the top/bottom plate and the side plate. The model predicted results was used as a guide to narrow down the micrograph sample area selections.

Ultrasonic testing was applied to qualitatively assess bonding status and cladding thickness/uniformity. Preliminary pulse-echo UT results based on the raw, unprocessed data indicate good bonding over most of the HIPped plates, with the exceptions of those noted. Qualitative results indicate some variation in the overall cladding thickness; a more thorough analysis and metallurgical correlation is required to calibrate in absolute numbers and to distinguish/account for Zr thickness and effects of residual stress and geometric distortions in the overall thickness measurement. Infrared thermography is a potential alternative to UT inspection for bond assessment; this would be an extremely fast measurement (several seconds vs 30 minutes/plate), however it may suffer from similar issues with regard to sample flatness and residual stress effects. In-house tests with existing equipment were unsuccessful due to a) insufficient vacuum within the cryo-cooling system (a maintenance issue) and b) a lens that was not optimally matched for the intended measurement. Newer commercially-available IR cameras, particularly those that incorporate Thermal Wave Imaging's patented Thermographic Signal Reconstruction (TSR) technology, appear well-suited to the HIPped plate bonding assessment application.

Three (3) bulge specimens were machined from Al/Zr/DU-10wt%Mo plate (ID: 529-1). The variation of applied pressure P as a function of the overall deflection of the deforming bulge δ was measured. This program also identified the bulge boundary or the location of the interfacial crack front. The local maxima of κ_{mean} is identified for all $0 \leq \theta \leq 2\pi$, and the closed loop of such local maxima is shown in the contour plot for κ_{mean} as dashed line as well. Detectable amount of delamination of the Al/Zr/DU-10wt%Mo interface is captured from the bulge boundaries. This program have successfully measured quantitatively the energy for creating new surface along the Al/Zr/DU-10wt%Mo interface In the meantime, this program had determined the area of the newly formed surface due to delamination of the Al/Zr/DU-10wt%Mo interface. The major portion of the data follow a straight line for $\Pi > 0$. The energy-release rate for the

stable extension of the Al/Zr/DU-10wt%Mo interfacial crack can be calculated to be 6.2 mJ/mm^2. The overall responses of the three specimens are quite similar for the applied hydraulic pressure P is plotted against the maximum deflection of the deforming bulge δ. Also the maximum pressure indicates that the interfacial strength of this Al/Zr/DU-10wt%Mo plate is relatively high compared to the other Al/Zr/DU-10wt%Mo plates we have tested so far. The fracture toughness results from the three bulge tests are consistent. Overall the bulge test results indicate that the Al/Zr/DU-10wt%Mo plate we tested has a relatively high toughness.

Metallography was used to exam any microstructural anomalies in the plate, foil, and along the fuel-clad interface. The bonding between LEU-Zr, Zr-Al, and Al-Al are well bonded without any crack, defect, or delamination. The interfaces are nice and clean without any distortion or pitting, which results in a nice and flat LEU foil. The middle section of the plate also indicates that the bonding between LEU-Zr, Zr-Al, and Al-Al are well bonded without any crack, defect, or delamination, which confirms that the whole plate has a consistence bonding from one end to the other. The higher magnification shows the thickness of the zirconium cladding as well as the clear well bonding between LeU-Zr and Zr-Al. Also, the Al-Al bond line can be seen from the left hand bottom corner of the micrograph. The Al-Al bonding has a well bonded interface showing a nice and smooth interface without any unbonded interface or any delamination. Metallography has demonstrated that no debonding in these fuzzy area from the ultrasonic testing, therefore the conclusion is that residual stress was the reason for the "fuzzy" data.

ACKNOWLEDGEMENTS

The authors would like to acknowledge the financial support of the U.S. Department of Energy (DOE) National Nuclear Security Administration (NNSA) Office of Material Management and Minimization (M^3) Reactor Conversion Program. Los Alamos National Laboratory, an affirmative action equal opportunity employer, is operated by Los Alamos National Security, LLC, for the NNSA of the U.S. DOE under contract DE-AC52-06NA25396.

REFERENCES

1. G. Moore "Rolling Studies Update Findings and Best Practices", May 2014, INL_MIS 14 32164.pdf

2. G. A. Moore, B. H. Rabin, J-F., Jue, C. R. Clark, N. E. Woolstenhulme, B. H Park, S. E. Steffler,M. D. Chapple, M. C. Marshall, J. J. Green, and B. L. Mackowiak, "DEVELOPMENT STATUS OF U10MO MONOLITHIC FUEL FOIL FABRICATION AT THE IDAHO NATIONAL LABORATORY" RERTR 2010, October 10-14, 2010, Lisbon, Portugal

3. , J. Katz, K. Clarke, B. Mihaila, J. Crapps, B. Aikin, V. Vargas, R. Weinberg, A. Duffield, D. Dombrowski, "Scale-Up of the HIP Bonding Process for Aluminum Clad LEU Reactor Fuel" RERTR 2011, October 23-27, 2011, Santiago, Chile

4. K.D. Clarke, C.E. Cross, R.E. Hackenberg, R.J. McCabe, J.D. Montalvo, M.J. Dvornak, R.L. Edwards, J.M. Crapps, R.R. Trujillo, B. Aikin, V.D. Vargas, K.J. Hollis, T.J. Lienert, B. Mihaila, D.L. Hammon, R.W. Hudson, T.J. Tucker, J.E. Scott, A.N. Duffield, R.Y. Weinberg, D.E. Dombrowski, "Development of Aluminum-Clad Fuel Plate Processing Through Canned and Canless Hot Isostatic Pressing (HIP), and Studies of Aluminum Cladding Grain Growth during HIP", RERTR 2012, October 14-17, 2012, Warsaw, Poland

5. J. Crapps, K. Clarke, J. Katz, D. Alexander, B. Aikin, V. Vargas, J. Montalvo, D. Dombrowski, B. Mihaila, Development of the hot isostatic press manufacturing process for monolithic nuclear fuel, Nuclear Engineering and Design 254 (2013) 43– 52

6. R. Edwards, M.A. Hill, R. K. Schulze, LEU Fuel Fabrication Process Cleaning Study Process Certification for Material Surface Cleaning for Bonded LEU Fuel Composite Including AFIP-7 LEU Coupons, LA-UR-11-02854, 2011